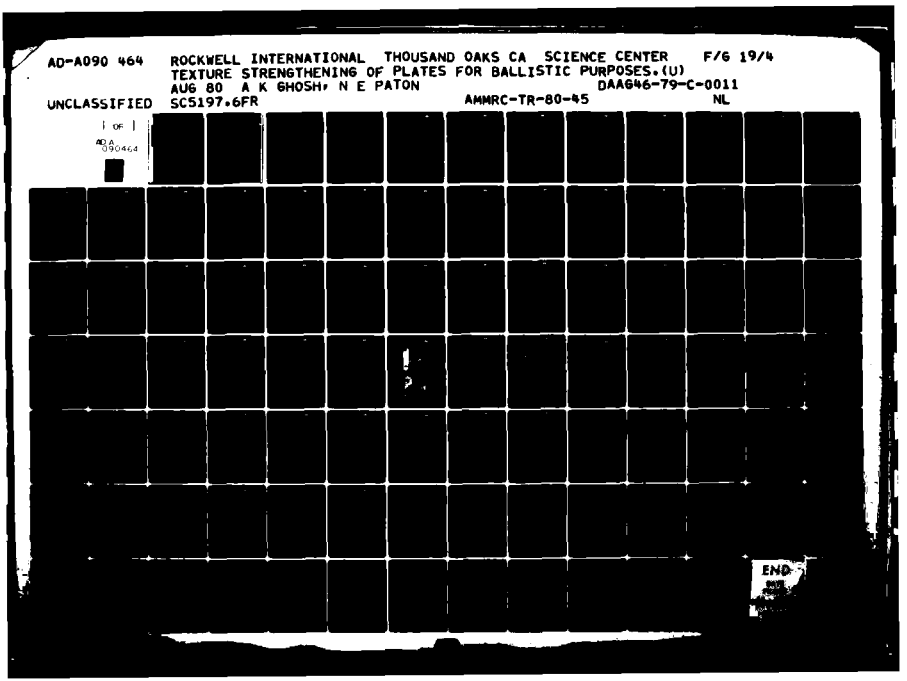
AD-A090 464
ROCKWELL INTERNATIONAL THOUSAND OAKS CA SCIENCE CENTER F/G 19/4
TEXTURE STRENGTHENING OF PLATES FOR BALLISTIC PURPOSES.(U)
AUG 80 A K GHOSH, N E PATON DAAG46-79-C-0011
UNCLASSIFIED SC5197.6FR AMMRC-TR-80-45 NL
1 OF 1
AD A 090464
END

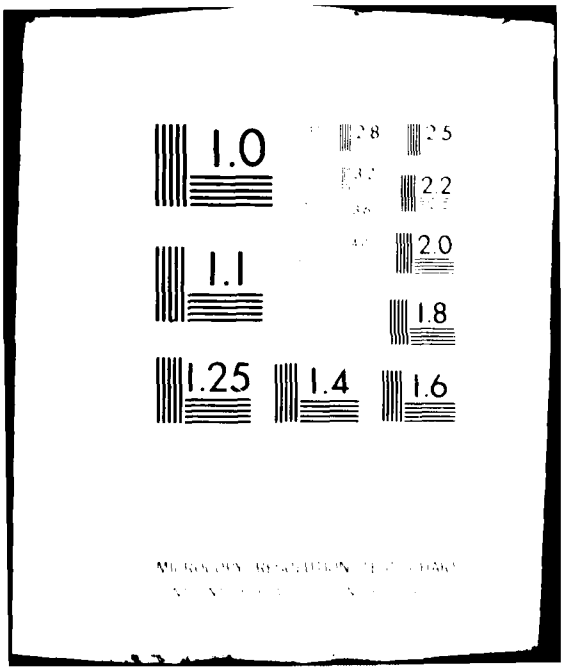
1.0
1.1
1.25
1.4
1.6
1.8
2.0
2.2

9

AMMRC TR 80-45

TEXTURE STRENGTHENING OF PLATES FOR BALLISTIC PURPOSES

August 1980

A. K. Ghosh and N. E. Paton
Rockwell International Corporation
Science Center
1049 Camino Dos Rios
Thousand Oaks, California 91360

Final Report

Contract Number DAAG46-79-C-0011

Prepared for

ARMY MATERIALS AND MECHANICS RESEARCH CENTER
Watertown, Massachusetts 02172

The findings in this report are not to be construed as an official Department of the Army position, unless so designated by other authorized documents.

Mention of any trade names or manufacturers in this report shall not be construed as advertising nor as an official indorsement or approval of such products or companies by the United States Government.

DISPOSITION INSTRUCTIONS

Destroy this report when it is no longer needed.
Do not return it to the originator.

UNCLASSIFIED

SECURITY CLASSIFICATION OF THIS PAGE (When Data Entered)

REPORT DOCUMENTATION PAGE

READ INSTRUCTIONS BEFORE COMPLETING FORM

1. REPORT NUMBER: AMMRC TR-80-45	2. GOVT ACCESSION NO.: AD-A090 464
3. RECIPIENT'S CATALOG NUMBER:	
4. TITLE (and Subtitle): Texture Strengthening of Plates for Ballistic Purposes	5. TYPE OF REPORT & PERIOD COVERED: Final Report 12/19/78 thru 03/18/80
6. PERFORMING ORG. REPORT NUMBER: SC5197.6FR	
7. AUTHOR(s): K. Ghosh & N. E. Paton (Amit)	8. CONTRACT OR GRANT NUMBER(s): DAAG46-79-C-0011
9. PERFORMING ORGANIZATION NAME AND ADDRESS: Rockwell International Corporation, Science Center, 1049 Camino dos Rios, Thousand Oaks, CA 91360	10. PROGRAM ELEMENT, PROJECT, TASK AREA & WORK UNIT NUMBERS: D/A Proj: 1L162105AH84, AMCMS Code: 612105.8H4.0011
11. CONTROLLING OFFICE NAME AND ADDRESS: Army Materials & Mechanics Research Center, Watertown, Mass. 02172	12. REPORT DATE: August 1980
	13. NUMBER OF PAGES: 86
14. MONITORING AGENCY NAME & ADDRESS (if different from Controlling Office)	15. SECURITY CLASS. (of this report): Unclassified
	15a. DECLASSIFICATION/DOWNGRADING SCHEDULE: N/A

16. DISTRIBUTION STATEMENT (of this Report)
Approved for public release; distribution unlimited

17. DISTRIBUTION STATEMENT (of the abstract entered in Block 20, if different from Report)

18. SUPPLEMENTARY NOTES

19. KEY WORDS (Continue on reverse side if necessary and identify by block number)

Texture
Preferred orientation
Alloy steel
Aluminum alloy
Deformation
Ballistics

20. ABSTRACT (Continue on reverse side if necessary and identify by block number)

Motivated by previous studies in relating texture-based strength to ballistic performance of 5% Ni steel armor, an investigation was initiated to examine other materials, particularly face-centered cubic materials, for possible texture strengthening effects. Theoretical and experimental work were carried out side by side, and significant progress in understanding and achieving that goal are reported here. On the theoretical side, (110) and (111) textures were identified as the most strong contributors to through-thickness strength, and →

DD FORM 1 JAN 73 1473 EDITION OF 1 NOV 65 IS OBSOLETE

UNCLASSIFIED

SECURITY CLASSIFICATION OF THIS PAGE When Data Entered

hence ballistic resistance. A computer program to calculate Taylor factors from pole figure data by incorporating spatial crystallite orientation distribution function was developed. Furthermore, theoretical modeling of the ballistic perforation process (~~Section 5~~) validated the previously speculated effects of normal anisotropy as well as showed the effects of other material properties, including strain hardening and strain-rate sensitivity. The experimental work on 7039 aluminum indicated only a weak texture, and relative absence of anisotropy leading to an absence significant ballistic effects. (Possibilities of altering this situation has been suggested in the text). Precipitation hardenable austenitic steel, A-286 grade, also used in this work, does give rise to "brass type" texture in rolled (at 80° and 900°F) and aged condition and appears to have a high through-thickness strength needed for ballistic resistance.

FOREWORD

This report was prepared by the Rockwell International Science Center under U.S. Army Contract No. DAAG46-79-C-0011. The research was conducted as part of a cooperative program in which U.S. Steel Research Laboratories had dveloped high strength armor plates, the deformation mechanics of which was studied at the Science Center. The contract was administered by the U.S. Army Materials and Mechanics Research Center, Watertown, Ma., Mr. Anthone Zarkades, Contracting Officer Representative. This is a final report and covers work conducted from December 19, 1978 to March 18, 1980.

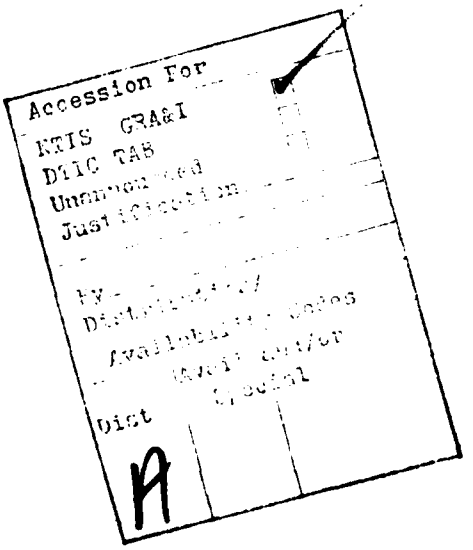

TABLE OF CONTENTS

LIST OF FIGURES

LIST OF FIGURES

LIST OF TABLES

TEXTURE STRENGTHENING OF PLATES FOR BALLISTIC PURPOSES

ABSTRACT

Motivated by previous studies in relating texture-based strength to ballistic performance of 5% Ni steel armor, an investigation was initiated to examine other materials, particularly face-centered cubic materials, for possible texture strengthening effects. Theoretical and experimental work were carried out side by side, and significant progress in understanding and achieving that goal are reported here. On the theoretical side, (110) and (111) textures were identified as the most strong contributors to through-thickness strength, and hence ballistic resistance. A computer program to calculate Taylor factors from pole figure data by incorporating spatial crystallite orientation distribution function was developed. Furthermore, theoretical modeling of the ballistic perforation process (Section 5) validated the previously speculated effects of normal anisotropy as well as showed the effects of other material properties, including strain hardening and strain-rate sensitivity. The experimental work on 7039 aluminum indicated only a weak texture and, relative absence of anisotropy leading to an absence significant ballistic effects. (Possibilities of altering this situation has been suggested in the text). Precipitation hardenable austenitic steel, A-286 grade, also used in this work, does give rise to "brass type" texture in rolled (at 80° and 900°F) and aged condition and appears to have a high through-thickness strength needed for ballistic resistance.

1.0 INTRODUCTION

Based on a study of texture-based strength of steels completed in late 1978,[1] a rationale was developed to relate preferred crystallographic orientation, and therefore, through-thickness strength anisotropy to ballistic performance. It was suggested that the first onset of deformation in the ballistic penetration process occurs by through-thickness compression and hence the strength in this deformation mode primarily controls penetration resistance. This rationale was found to explain the V_{50} ballistic behavior of a medium carbon 5% Ni-Si-Cu-Mo-V steel manufactured by U.S. Steel,[2] specifically to develop high intensities of (112) and (111) textures. Calculation of Taylor factor, M, for various ideal textures also showed that highest through-thickness strength would be expected in the case of these textures.

A detailed study by Zarkades[3] shows quantitatively the improvement in penetration resistance as a function of texture intensity. This is further supported by the superiority in the weight merit ratio (a real density ratio for the same penetration resistance) of textured steel over the isotropic material. The textured steel also exhibited superior fracture toughness over isotropic material and a large anisotropy in fatigue endurance limit, tensile properties, impact energy, etc., in the plane of the plate.

Based on these positive results, a systematic study was initiated in the past year to examine other material systems for improved texture-based strength properties. The crystal structure of particular interest here is face-centered cubic materials. Since a number of armored vehicles use 7039

aluminum alloy, it is of interest to know if texture would influence its strength or fracture characteristics. Furthermore, there are a number of precipitation hardenable high strength austenitic steels that could compete with 4340 or 5% Ni-Steels in terms of strength properties. A-286 steel, a highly creep resistant material is an excellent example. The possibility of developing texture-based strength in such an f.c.c. material is thus interesting and challenging. In this connection, the calculation of Taylor factors for various ideal crystallographic orientations for f.c.c materials, is essential for a preassessment of the expected behavior.

The studies on Taylor factors based on ideal orientations are somewhat subjective since real material plate textures have three-dimensional distribution of orientations associated with them. A more realistic strength prediction should include this distribution as well. Based on existing literature work, a capability needs to be developed to incorporate 3-D orientation distributions in such calculations, particularly for comparison with results based on ideal orientations. In the work described here, a computer program was developed with the consulting help of Prof. John Kallend of Illinois Institute of Technology, for calculating Taylor factors from two (for cubic materials) complete pole figure data.

In addition to seeking answers to these questions, two other related topics are investigated because of their extreme importance to this program. One relates to the elevated temperature fabrication of components from the superior 5% Ni armor steel. The concern is if the elevated temperature exposure causes any damage to the mechanical properties of the steel. The

other topic, treated in Section 5.0, deals with an analytical approach to looking at the influenece of material's plastic properties, including its strain-hardening, strain-rate sensitivity and anisotropy effects on ballistic penetration process. This is an essential part of plate strengthening program for ballistic purposes.

2.0 TAYLOR FACTORS (M) FOR F.C.C. MATERIALS

Background

Strengthening of sheets and plates by altering their crystallographic texture through various thermomechanical processing techniques is a subject of continuing interest. In b.c.c. metals like iron and steel texture strengthening in the through-thickness direction (of plates) is achieved by aligning as many (111) planes parallel to the rolling plane as possible. Hu, Speich and Miller[2] have taken advantage of this principle in the manufacture of armor plates of 5% Ni-Si-Cu-Mo-V steel steel. These are primarily martensitic plates with varying amounts of rolling reduction to impart varying degrees of texture intensities. They reported significant ballistic improvements with (111) and (112) textures.

The analytical and experimental work carried out during the last year[1] showed that through-thickness strength is highly instrumental in controlling ballistic perforation resistance. The obvious question is then if this technique could be used in other crystallographic systems to improve ballistic performance. Since high strength aluminum is being used in some armored vehicles at the present time there is interest in studing texture strengthening of such an aluminum alloy. Other f.c.c. steels, e.g., austenitic stainless or precipitation hardened austenitic steels could also be used for the study. In conjunction with this there is the need for calculating texture based strength to see which ideal textures might be worth investigating. Of course, there may still remain the problem of actually

producting a strong rolling texture in a f.c.c. material. We are quite fortunate with body-centered cubic materials in this respect that pencil glide provides these materials with a single slip direction (111) and the texture can be sharpened. Strong recrystallization texture (100) can, however, be produced in f.c.c. materials and deformation texture in h.c.p. materials.

The work of Taylor[4] and Bishop and Hill[5] are extensively used for calculating texture-based strength. The method for calculating Taylor factor, M (ratio of yield strength to critical resolved shear stress for slip), popularized by Hosford and Backofen[6] and Chin and co-workers,[7-9] for various ideal crystal orientations, has primarily been applied to uniaxial tension or compression modes of deformation. In ballistic impact, virtual absence of acceleration[10] gives rise to deformation modes that are either through-thickness compression (identical to balanced biaxial tension in the plane of the sheet) or shear. Therefore, M factors for these deformation modes were calculated.

Even though the strain-rates for ballistic penetration are extremely high, deformation is still believed to occur by crystallographic slip and hence the need for a crystallographic approach. The calculation of M factors as a function of test direction for various ideal textures can also indicate if failure might occur in a shear mode or by petalling or back spalling. It is therefore, important to develop such information to guide the production of steel plates for a desired kind of ballistic resistance.

Approach

The analytical approach for texture based strength calculations have been detailed in last year's report.[1] The method is that of Bishop and Hill and consists of converting an imposed shape change on the plate to crystallographic shear directions and calculating deformation resistance from the knowledge of slip shear resistance. A brief summary of this method is given below:

Figure 1 relates the impact direction to the sheet directions: rolling (r), transverse (t) and thickness (z). The direction cosines between the impact direction (a_1, a_2 and a_3) and sheet directions are expressed as follows:

	a_1	a_2	a_3
t	cos θ sin α	-sin θ	-cos θ cos α
r	sin θ sin α	cos θ	-sin θ cos α
z	cos α	0	sin α

Writing 1, 2 and 3 in places of a_1, and a_2 and a_3, the imposed shape changes for through thickness compression are

$$d\varepsilon_3 = -2d\varepsilon_1 = -2d\varepsilon_2;\ d\varepsilon_{12} = d\varepsilon_{23} = d\varepsilon_{31} = 0; \qquad (1)$$

and planar shear are

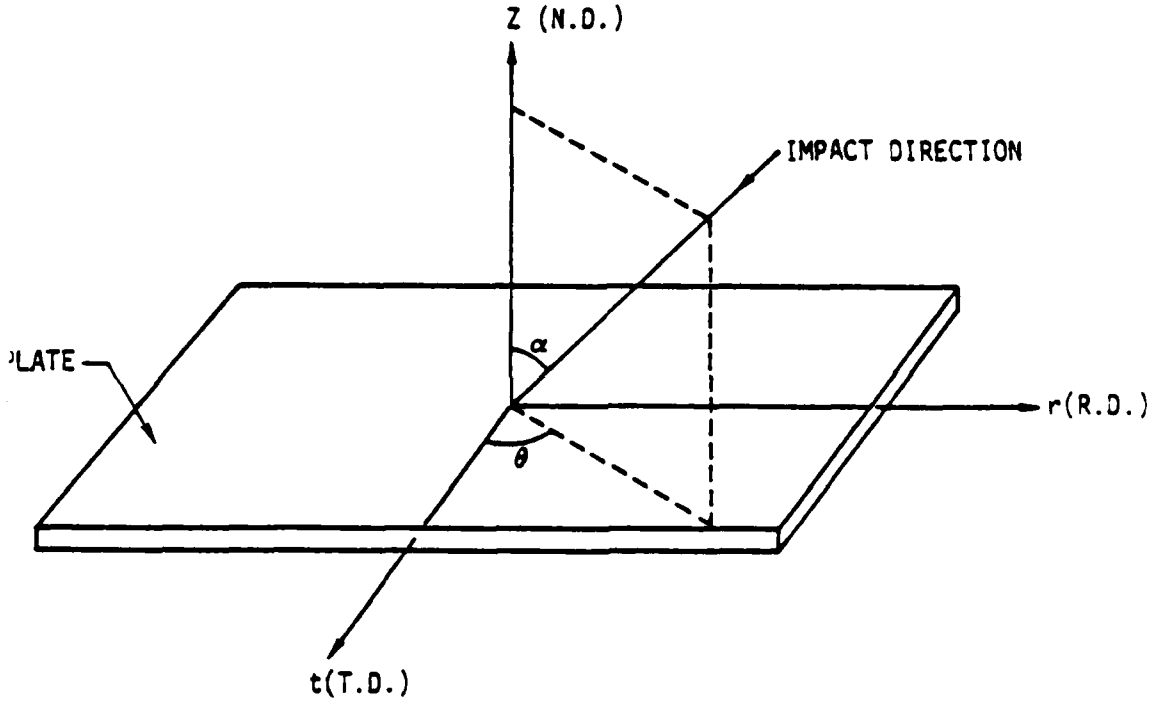

Fig. 1 Relationship between impact directions and the orthogonal directions of the plate.

$$d\gamma_{21} \neq 0;\ d\gamma_{31} = d\varepsilon_1 = d\varepsilon_2 = d\varepsilon_3 = d\gamma_{23} = 0, \qquad (2)$$

noting that $\gamma_{21} = 2\varepsilon_{21}$ etc., where γ = imposed shear strain and ε = component of the imposed strain tensor.

After these shape changes are resolved[4] in the sheet directions using the above direction cosines, they are resolved in the crystal directions (100), (010) and (001) for each ideal orientation. Table 1 lists the ideal f.c.c. rolling textures found experimentally. The simplest texture is (110) $[1\bar{1}2]$, however, (123) $[1\bar{2}1]$ is extremely common and may be thought to be composed of (110) and (112) textures. As a reminder, a combination (111) and (112) textures were found in the strong armor plates of Hu et al.[2] The direction cosines between the crystallographic directions and the sheet directions are used in the last transformation scheme.

Knowing the shape change in the crystal direction allows us to use Bishop and Hill stress-states for (111) <110> slip system for f.c.c. materials for maximizing the virtual work. These stress-states are given by $A = (\sigma_2 - \sigma_3)/\sqrt{6}\,\tau_s$, $B = (\sigma_3 - \sigma_1)/\sqrt{6}\,\tau_s$, $C = (\sigma_1 - \sigma_2)/\sqrt{6}\,\tau_s$, $F = \sigma_{23}/\sqrt{6}\,\tau_s$, $G = \sigma_{31}/\sqrt{6}\,\tau_s$ and $H = \sigma_{12}/\sqrt{6}\,\tau_s$, which can take values of 0, $\pm$ 1/2 and $\pm$ 1, the stresses being taken with reference to the cube axes, τ_s = critical resolved shear stress. M, which is given by $dW/\tau_s d\gamma$ for shear and $dW/\tau_s d\varepsilon_3$ for through-thickness compression is obtained by finding the maximum value of

$$M = \sqrt{6}\left[-B\frac{d\varepsilon_1}{d\varepsilon} + A\frac{d\varepsilon_2}{d\varepsilon} + 2F\frac{d\varepsilon_{23}}{d\varepsilon} + 2G\frac{d\varepsilon_{21}}{d\varepsilon} + 2H\frac{d\varepsilon_{12}}{d\varepsilon}\right] \qquad (3)$$

from the 28 possible combinations of A, B....H ($d\varepsilon_{31}$ stands for $d\gamma/2$ or $d\varepsilon_{13}$). A FORTRAN computer program was written to compute M and the results are discussed subsequently.

Table 1

Ideal Rolling Textures In
f.c.c. Materials

Cu	(110)/[1$\bar{1}$2]
Cu	(123)/[1$\bar{2}$1]
Cu	(123)/[1$\bar{2}$1]
Cu 70% - Zn 30%	($\bar{1}$10)/[$\bar{1}$12]
Cu 70% - Zn 30%	($\bar{1}$10)/[$\bar{1}$12]
Cu + 12 at. % Al	(123)/[1$\bar{2}$1]
Cu + 1.5 at. % Al	($\bar{1}$10)/[$\bar{1}$12]
Cu + 3 at. % Au	(123)/[1$\bar{2}$1]
Cu + 29.6 at. % Ni	(123)/[1$\bar{2}$1]
Cu + 49 at. % Ni	(123)/[1$\bar{2}$1]
Ni	(123)/[1$\bar{2}$1]
Au	(123)/[1$\bar{2}$1]
Au + 10 at. % Cu	($\bar{1}$10)/[$\bar{1}$12]
Al	(123)/[1$\bar{2}$1]
Al	($\bar{1}$10)/[$\bar{1}$12]
Al + 2 at. % Cu	(110)/[1$\bar{1}$2]
Al + 1.25 at. T Si	(123)/[1$\bar{2}$1]
Al + 0.7 at. % Mg	(110)/[1$\bar{1}$2]
Ag	(110)/[1$\bar{1}$2]
Pb + 2 wt % Sb	(110)/[011]

Results

In the results to be presented, the Taylor factors (M) for the various ideal textures are normalized with respect to M for random crystal orientation. In the (110) pole figures for 5% Ni steel,[2] a 13° rotation about the transverse direction of a (111) $[11\bar{2}]$ texture was found to describe the intensity maxima better than (111) $[11\bar{2}]$ texture itself. Strength calculations were carried out for this 13° rotated texture and compared with b.c.c. (111) $[11\bar{2}]$ texture in Figs. 2 and 3 as normalized with respect to random texture. While through-thickness strength is reduced on account of the rotation, the shear strength in the rolling direction is significantly increased, thus producing a strength anisotropy. This effect might be responsible for the preferential penetrator exit direction observed from tests conducted on these plates.

The calculated strength, for the f.c.c. textures are also shown in Figs. 2 and 3. The (110) $[1\bar{1}2]$ texture appears to be the most promising (1.21 times random) with strength equivalent to that of the b.c.c. (111) texture. The (112) type texture for both b.c.c. and f.c.c. have the same strength, while (123) texture has the lowest strength (less than random) among these. Thus, the notion that the strength of (123) would be intermediate between (111) and (112) type textures is not valid. The shear strength values of all the textures are about the same (less than random), with (123) type showing a peak in the transverse direction.

SC79-4020

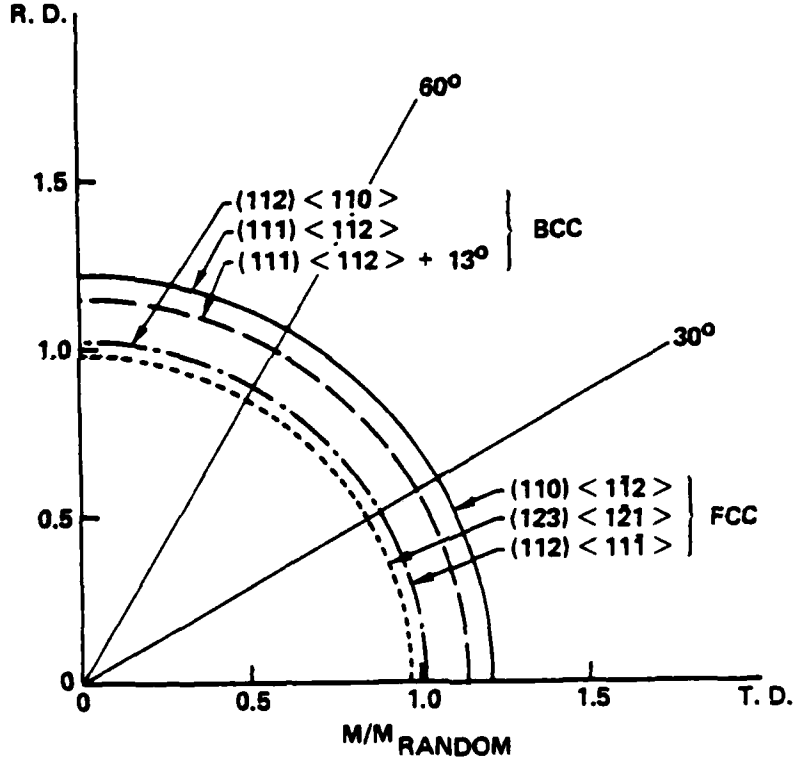

Fig. 2 Normalized Taylor factors for through-thickness compression.

SC79-4019

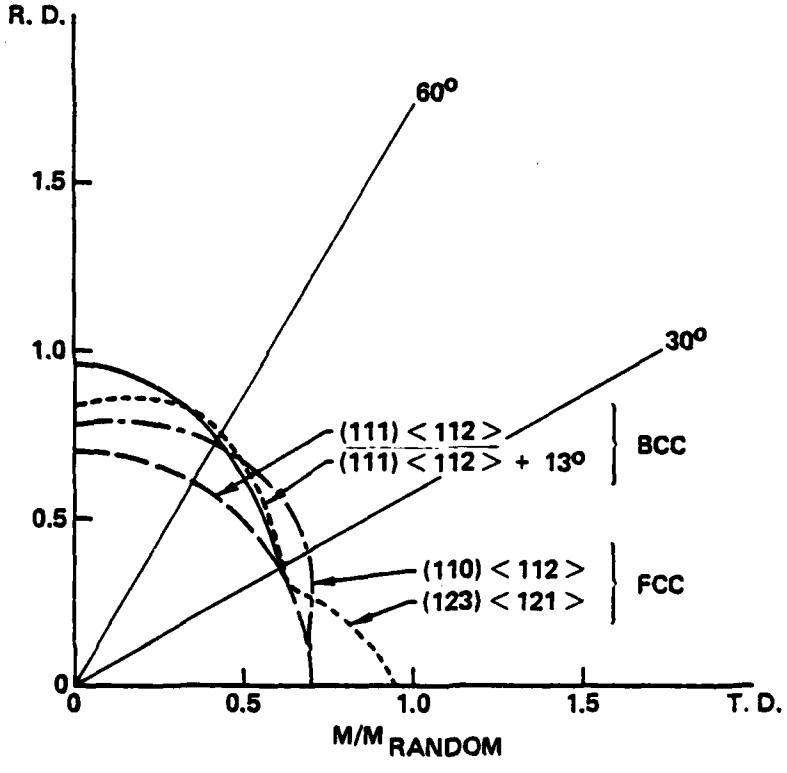

Fig. 3 Normalized Taylor factors for planar shear.

The (100) recrystallization texture for the f.c.c. metals is normally very strong. However, as shown in last year's report,[1] this texture is weak in compression (even though extremely strong in shear (see Figs. 4 and 5) and, therefore, not highly promising for ballistic resistance. Thus the f.c.c. texture that may be best from the standpoint of ballistic resistance is (110) $[1\bar{1}2]$ (or Brass type) if a strong component of this could be produced.

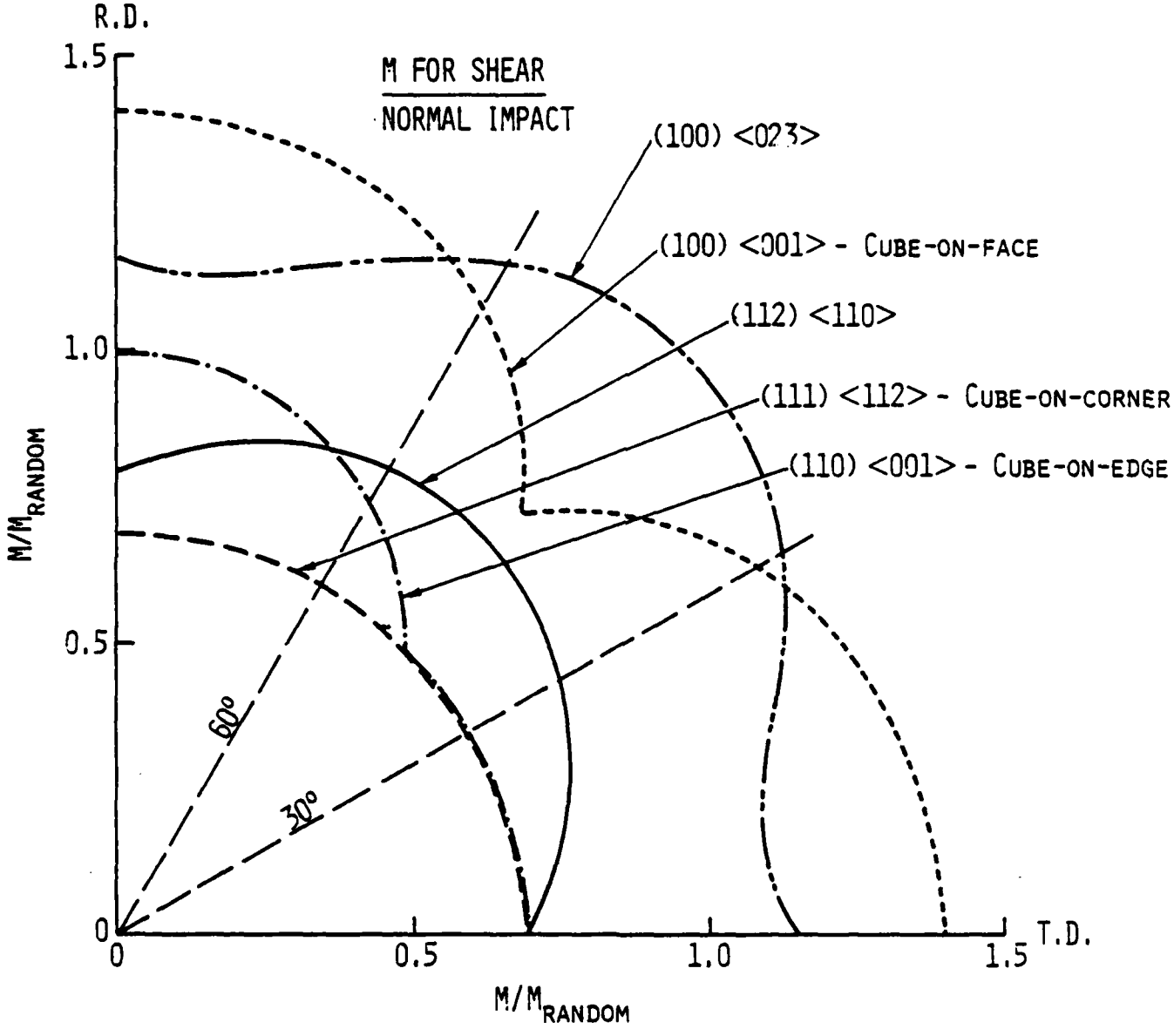

Fig. 4 Normalized Taylor factor for shear as a function of sheet direction (b.c.c. textures).

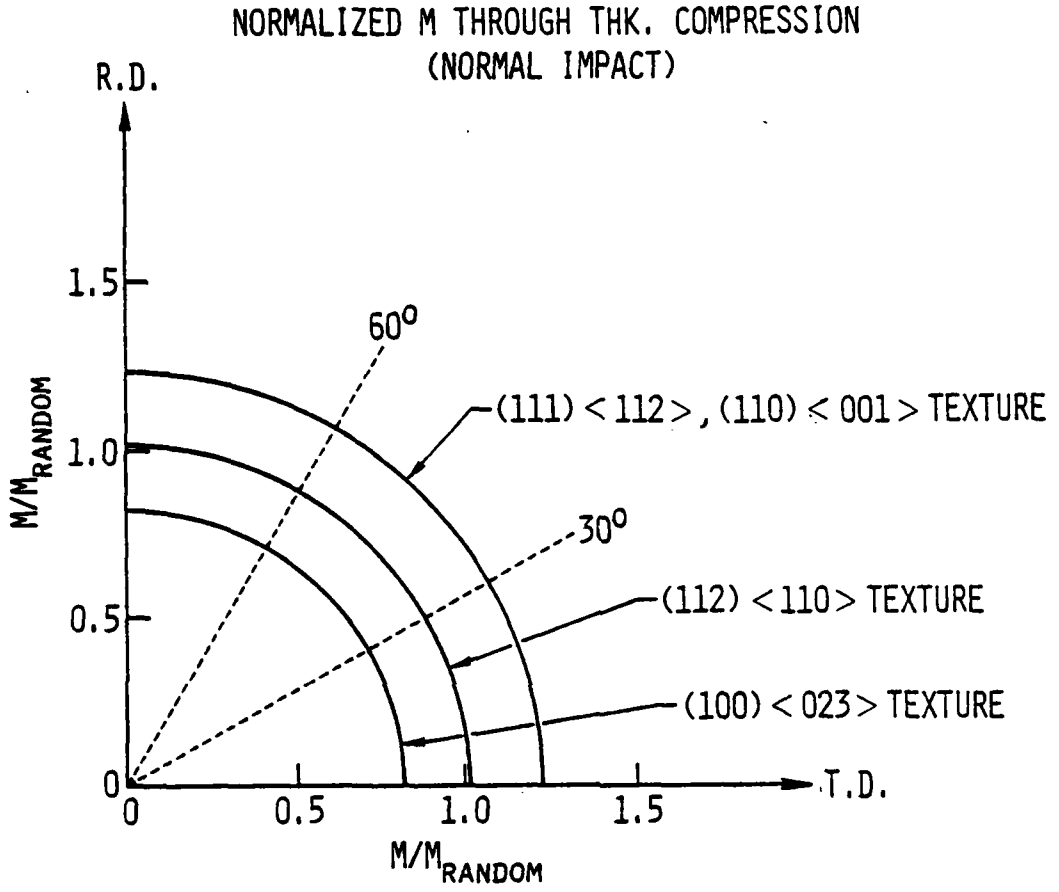

Fig. 5 Normalized Taylor factor for through-thickness compression (b.c.c. textures).

3.0 THREE DIMENSIONAL ORIENTATION DISTRIBUTION EFFECTS ON TEXTURE STRENGTH

Background

While the assigning of ideal orientations to describe plate texture promotes easier understanding of their influence on strength properties, it is by no means as accurate as the present-day techniques would allow. A pole figure shows significant intensity distribution around the observed pole maxima and is merely a reflection of its spatial distribution. In Fig. 6 a partial pole figure for 5% Ni steel[2] shows that neither (112) $[1\bar{1}0]$ nor a 13° rotation from (111) $[\bar{1}\bar{1}2]$ describe the details of the intensity distribution. To determine the effects of all orientations on strength and other mechanical properties, a description of three-dimensional crystallite orientation distribution is required.

The complete description of anisotropy has been achieved through crystallite orientation distribution function (CODF) by a number of investigators.[11-13] This function, $w(\theta, \phi, \psi)$ (where θ, ϕ and ψ are a set of Euler angles) may be used with an equivalent description of an anisotropic mechanical and physical property, $g(\theta, \phi, \psi)$, to predict orientation dependent properties. For a textured specimen, it is necessary to average work increment dw, for given imposed strain over all crystallite orientations and this requires that the contributions due to each crystallite orientation be weighted by the density of occupation of that orientation. This is what is described by a three dimensional spherical harmonic function and is derived from at least two complete pole figures for a cubic material.

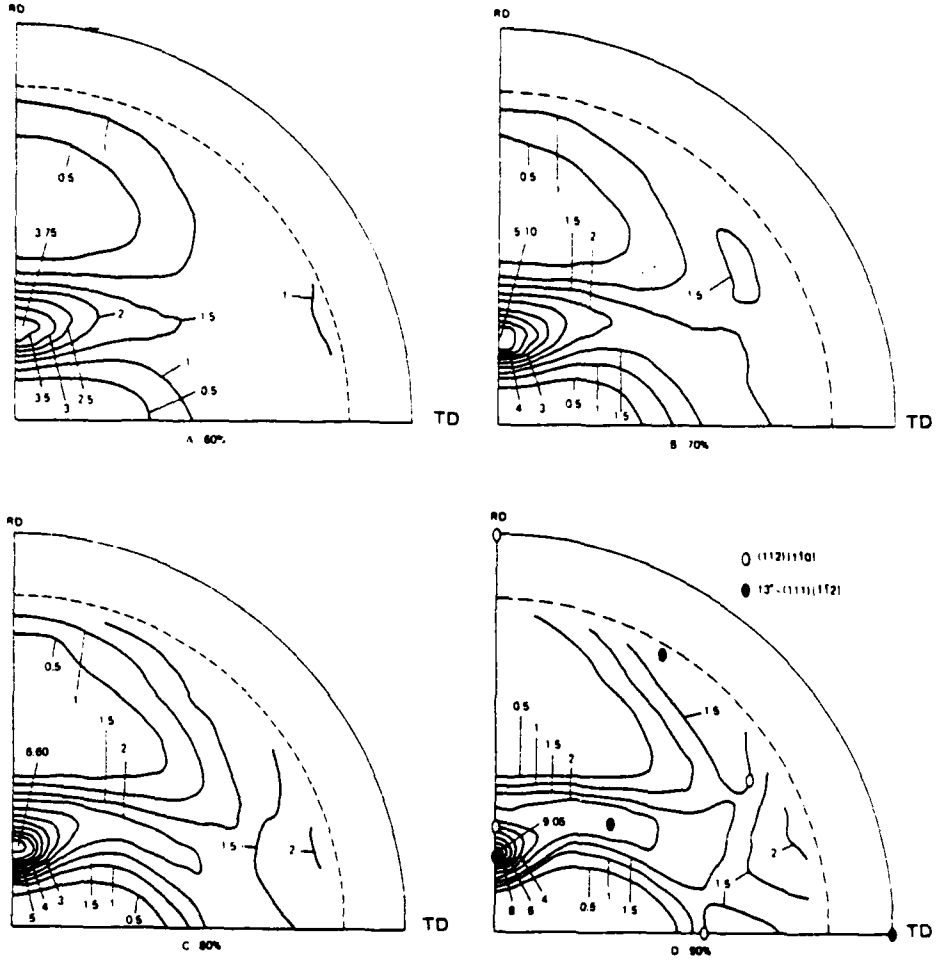

Fig. 6 (110) pole figures of 5% Ni plates rolled to various reductions at 1500°F, then quenched and tempered (from H. Hu, AMMRC Report CTR 77-19, July 1977).

To obtain the coefficients of the spherical harmonic function, let us suppose that the normalized pole figure intensity at an angular coordinate position, (α, β) on the pole figure is $q(\alpha, \beta)$. If the intensity distribution is describable by means of a spherical harmonic function $P_{lm}(\beta)\, e^{-im\alpha}$, and Q_{lm} are coefficients, then by definition

$$q(\alpha, \beta) = \sum_{l=0}^{\infty} \sum_{m=-l}^{l} Q_{lm} P_{lm}(\beta)\, e^{-im\alpha} \tag{4}$$

Thus from the measured intensity values $q(\alpha, \beta)$, the coefficients can be determined as

$$Q_{lm} = \frac{1}{4\pi^2} \int_{all} \int_{\alpha,\beta} q(\alpha, \beta)\, P_{lm}(\beta)\, e^{-im\alpha}\, d\beta d\alpha \tag{5}$$

Similarly CODF represented by $w(\theta, \phi, \psi)$, is given by

$$w(\psi,\theta,\phi) = \sum_{l}^{\infty} \sum_{m=-l}^{l} \sum_{n=-l}^{l} W_{lmn} Z_{lmn}(\theta)\, e^{-im\psi}\, e^{-in\phi} \tag{6}$$

where W_{lm} are the coefficients to be determined and $Z_{lmn}(\theta)$ are augmented Jacobi polynomials. Then the coefficients Q_{lm} and W_{lmn} are related by a set of linear equations:

$$Q^j_{lm} = 2\pi \left(\frac{2}{2l+1}\right)^{1/2} \sum_{p=-l}^{l} W_{lmp} P_{lp}(\eta_j) e^{-ip\mu_j} \tag{7}$$

where η_j, μ_j are the polar coordinates of the plane normal of the diffracting plane for the j^{th} pole figure, with respect to the CRYSTAL axis.

Hence the Q_{lm} may be found by numerical integration of Eq. (5), and the W_{lmn} by solution of Eq. (7). The orientation distribution function can then be found by substitution in Eq. (6).

[In practice, for symmetrical specimen and crystal geometry, the exponential terms all reduce to cosine terms, and many of the Q_{Lm} and W_{Lmn} are identically equal to zero. Additionally,

$$Q_{lm} \equiv Q_{l\bar{m}}, \quad W_{lmn} = W_{l\bar{m}n} - W_{l\bar{m}\bar{n}}$$

and for given values of l and m, the W_{lmn} are linearly related. These conditions are built into the computer program.]

Once CODF is known, which acts as a weighting function, the next step is to determine a Taylor factor distribution function in terms of Euler angles. This is done by assuming a crystallite present at each Euler Angle orientation and calculating the corresponding Taylor factors for an imposed strain tensor. If this function is given by g (ψ, θ, ϕ), its average value for the polycrystalline aggregate is given by

$$\bar{g} = \int_{\substack{\psi\theta w \\ \text{all}}} \int\int w(\psi, \theta, w)\, g(\psi, \theta, x) \sin\theta \, d\phi \, d\theta \, d\psi \qquad (8)$$

If $g(\psi, \theta, \phi)$ is expanded as a series of spherical harmonics,

$$g(\psi, \theta, \phi) = \sum_{l} \sum_{m} \sum_{n} G_{lmn} Z_{lmn}^{(\theta)} e^{-im\psi} e^{-in\phi}$$

where the coefficients G_{lmn} are found by numerical integration. Equation (8) then becomes

$$\bar{g} = 4\pi^2 \sum_{l} \sum_{m} \sum_{n} W_{lmn} G_{lmn} \qquad (9)$$

For rotations of α about the specimen z axis (i.e., plate normal) the average Taylor factor may be determined from

$$\bar{g}(\alpha) = 4\pi^2 \sum_{l} \sum_{m} \sum_{n} W_{lmn} G_{lmn} \cos(m\alpha) \qquad (10)$$

Based on the above theoretical background, Prof. J. Kallend of Illinois Institute of Technology had developed computer programs, which were acquired at the Rockwell Science Center through his consulting services. Briefly, the program description is as follows:

Program CUBAN calculates Q_{lm} from pole figure data by numerical integration. The program also estimates the truncation error in the series expansion due to termination at a finite (usually 20) order. Program CODF calculates the crystal orientation distribution function coeffieients, W_{lmn}, from coefficients of the spherical harmonic series calculated by the CUBAN program.

Program PLASGEN determines the coefficients, G_{lmn}, for the orientation dependence of the Taylor factor for an imposed strain tensor which is supplied as data.

Finally, program PLASTIC reads in the coefficients G_{lmn} and W_{lmn}, and calculates the average Taylor factor according to Eq. (10).

3.1 Pole Figures of 7039 Al and Calculated Taylor Factors

7039 aluminum plate (1.5 in. thick) has important armor applications because of its high strength and corrosion resistance. The mechanical properties of this and other alloys are given in Section 4.0.

In this section the Taylor factor calculations based on actual crystallographic orientation distributations of this alloy is presented, following the procedure described in Section 3.0.

The crystallographic orientations of the 7039 aluminum armor plates have been characterized experimentally by their pole figures. From the 1.5 in. thick plate supplied by AMMRC, 1 in. x 6 in. x 0.10 in. strips were cut from near the surface and center, parallel to the rolling plane for this work. From 0.16 in. strip of the same material, which was rolled at AMMRC, 1 in. x 6 in. pieces were also cut. All of the test materials were sent to Boeing Technology Services in Seattle for the pole figure work. Figures 7(a), (b), 8(a), (b), and 9(a), (b) show, respectively, the (111) and (200) pole figures for 7039 surface, center (from 1.5 in. thick plate) and the rolled 7039 plate. F.c.c. ideal orientations corresponding to low index planes are

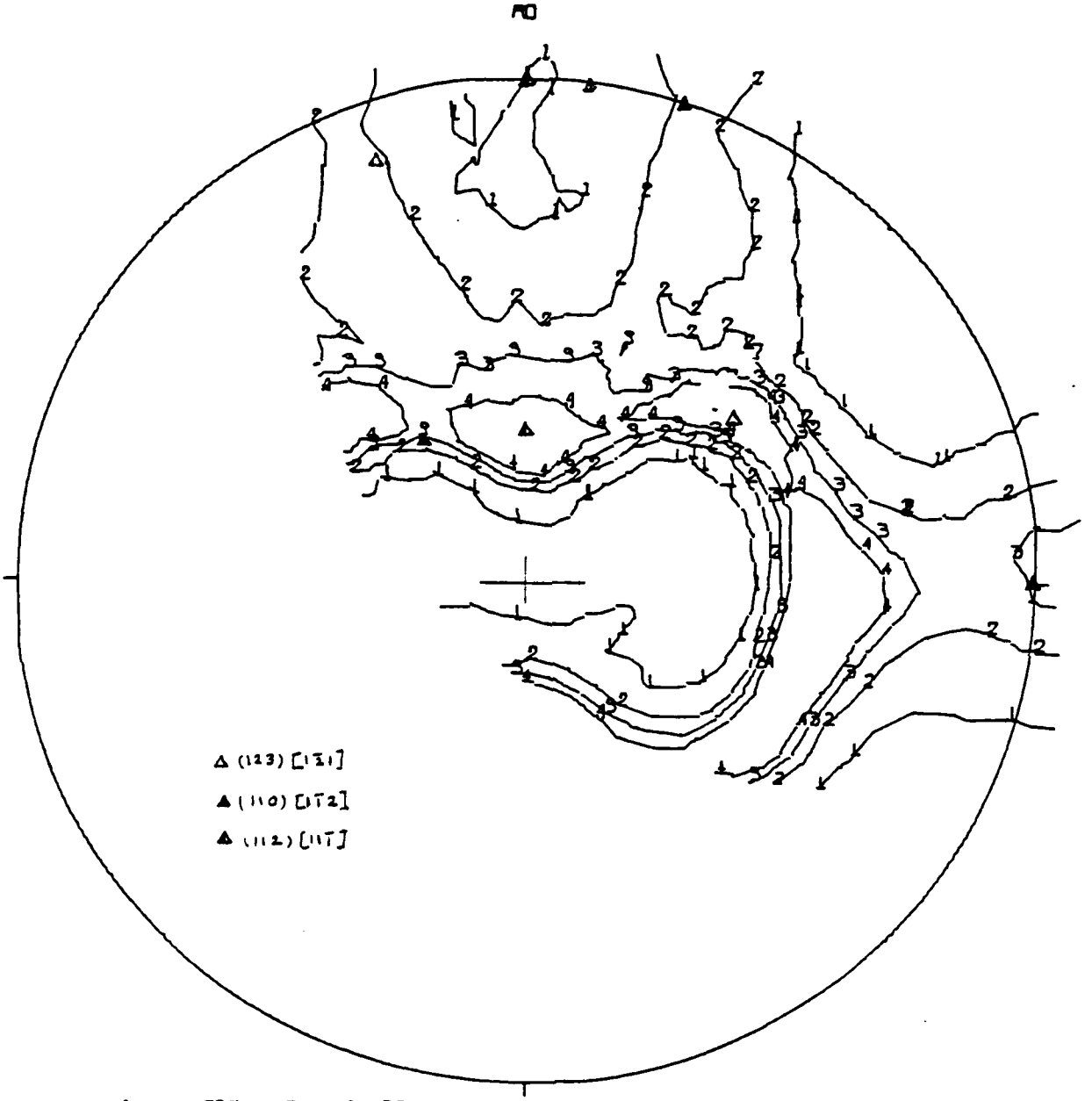

BMT JOB NO.79-01871 7039-0 ALUMINUM SURFACE DATE 05-SEP-79
RADIATION- CU AT 35KV/20MA COUNTER-PROPORTIONAL AT 2.000KV
SLITS- 2H/2V ENTRANCE, 5H/1V RECEIVING ENGINEER-DAVID G. EVANS
SCAN RATE- 1DEG/MIN, 72ALPHA/MIN HKL= 111
PHA- 25V BASE, 20V WINDOW SILVER CALIBRATION
RANDOM INTENSITY (CALC) 2068.1 RD= 45.00 FD= 54.74

Fig. 7(a) (111) pole figure of 7039 aluminum (surface).

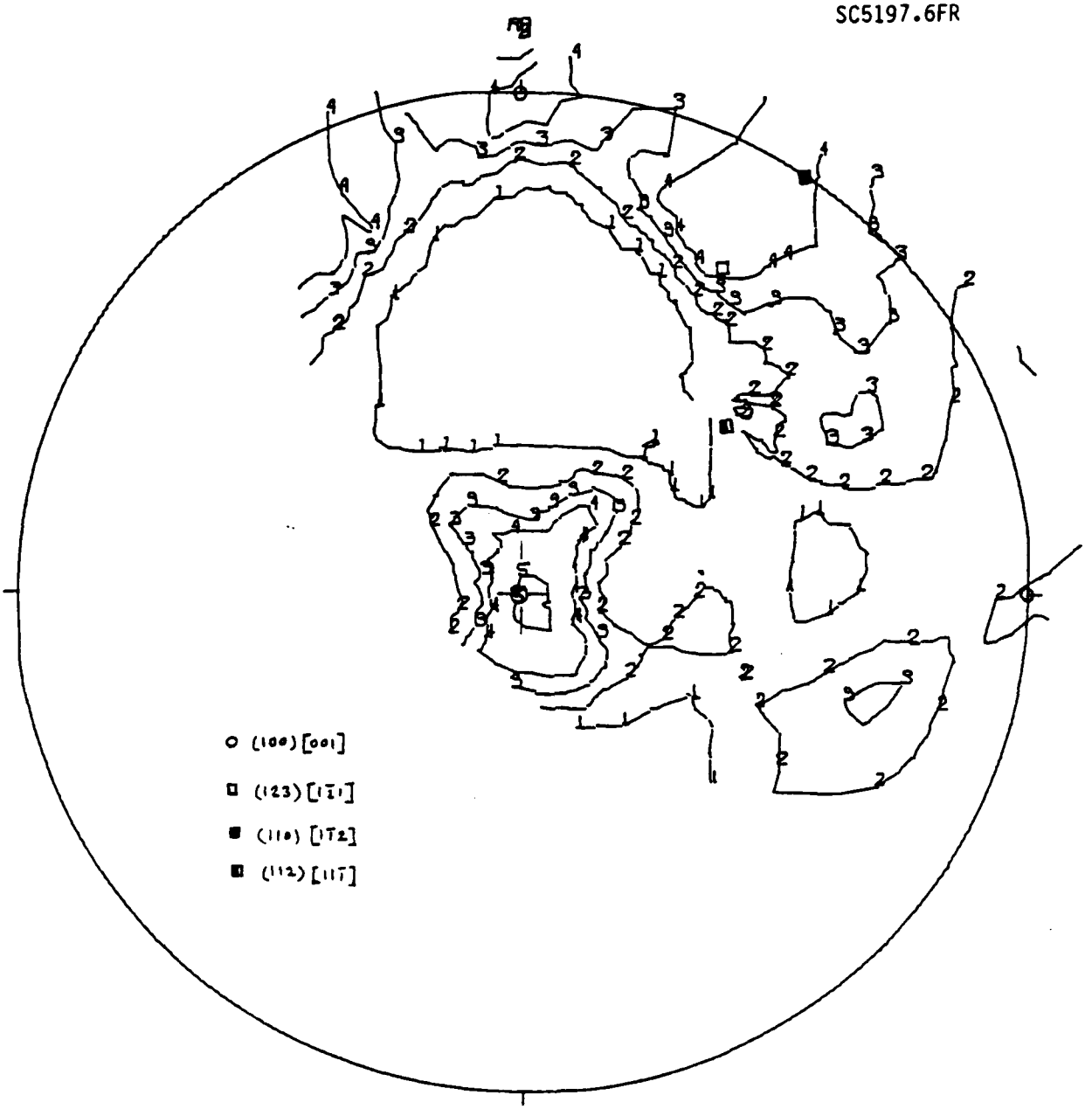

1	.500	2	1.000	3	1.500	4	2.000	5	4.000
6	8.000	7	14.000	8	20.000	9	25.000	0	30.000

BMT JOB NO.79-01871 7039-0 ALUMINUM.SURFACE DATE 06-SEP-79
RADIATION- CU AT 35KV/20MA COUNTER-PROPORTIONAL AT 2.000KV
SLITS- 2H/2V ENTRANCE, 5H/1V RECEIVING ENGINEER-DAVID G. EVANS
SCAN RATE- 1DEG/MIN, 72ALPHA/MIN HKL= 200
PHA- 25V BASE, 20V WINDOW SILVERCALIBRATION
RANDOM INTENSITY (CALC) 848.3 AO= 45.00 CO= 54.74

Fig. 7(b) (200) pole figure of 7039 aluminum (surface).

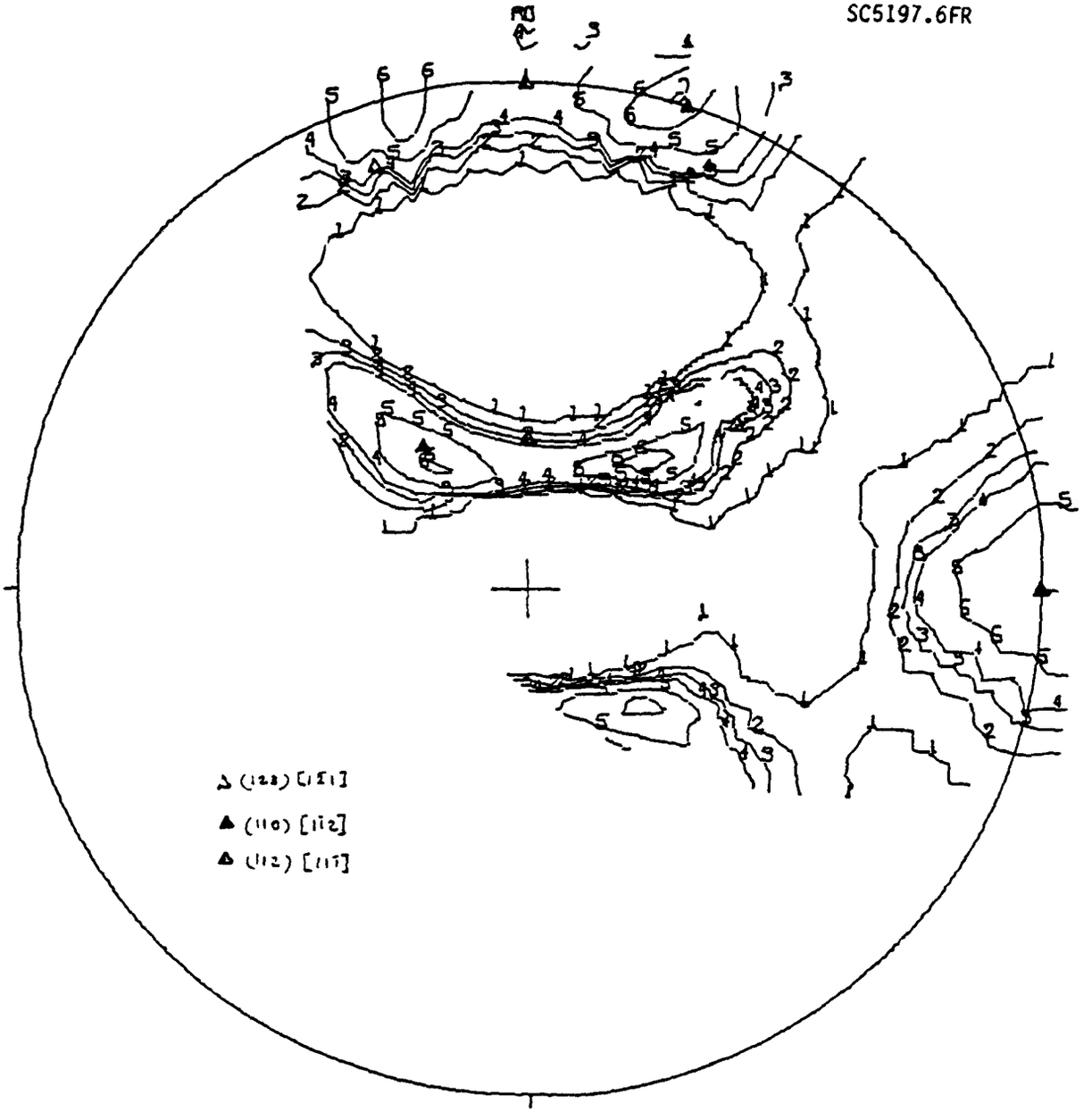

1	.500	2	1.000	3	1.500	4	2.000	5	4.000
6	8.000	7	14.000	8	20.000	9	25.000	0	30.000

BNT JOB NO.79-01871 7039-0 ALUMINUM.CENTER DATE 04-SEP-79
RADIATION- CU AT 35KV/20MA COUNTER-PROPORTIONAL AT 2.000KV
SLITS- 2H/2V ENTRANCE, 5H/1V RECEIVING ENGINEER-DAVID G. EVANS
SCAN RATE- 1°B1/MIN, 72ALPHA/MIN HKL= 111
PHA- 25V BASE, 20V WINDOW SILVER CALIBRATION
RANDOM INTENSITY (CALC) 1876.4 AO= 45.00 FO= 54.74

Fig. 8(a) (111) pole figure of 7039 aluminum (center).

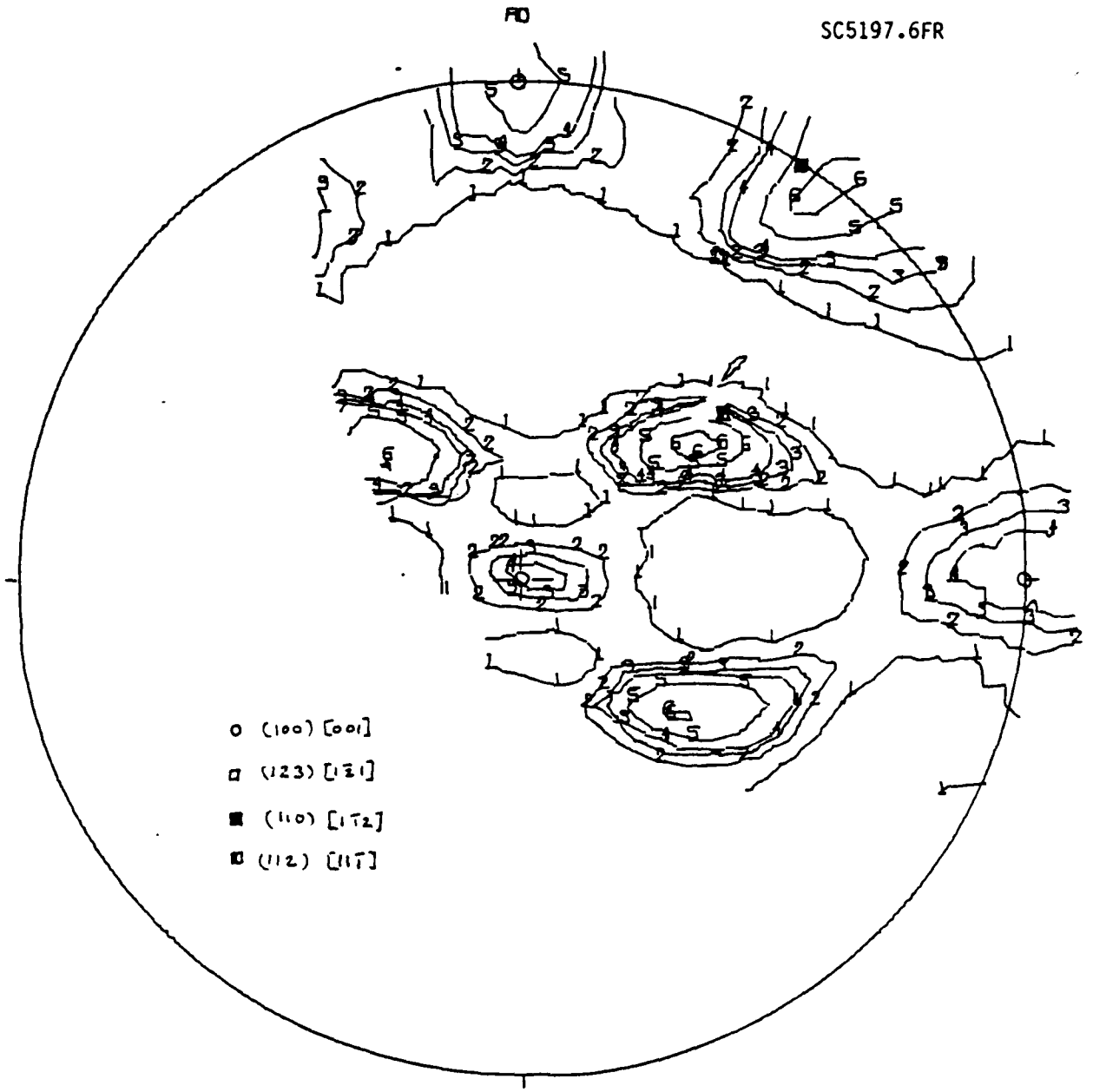

1	.500	2	1.000	3	1.500	4	2.000	5	4.000
6	8.000	7	14.000	8	20.000	9	25.000	0	30.000

ENT JOB NO.79-01871 7039-C ALUMINUM.CENTER DATE 04-SEP-79
RADIATION- CU AT 35KV/20MA COUNTER-PROPORTIONAL AT 2.000KV
SLITS- 2H/2V ENTRANCE, 5H/1V RECEIVING ENGINEER-DAVID C. EVANS
SCAN RATE- 1°61/MIN. 72ALPHA/MIN HKL= 200
PHA- 25V BASE. 20V WINDOW SILVER CALIBRATION
RANDOM INTENSITY (CALC) 866.1 RD=225.00 PD=-54.74

Fig. 8(b) (200) pole figure of 7039 aluminum (center).

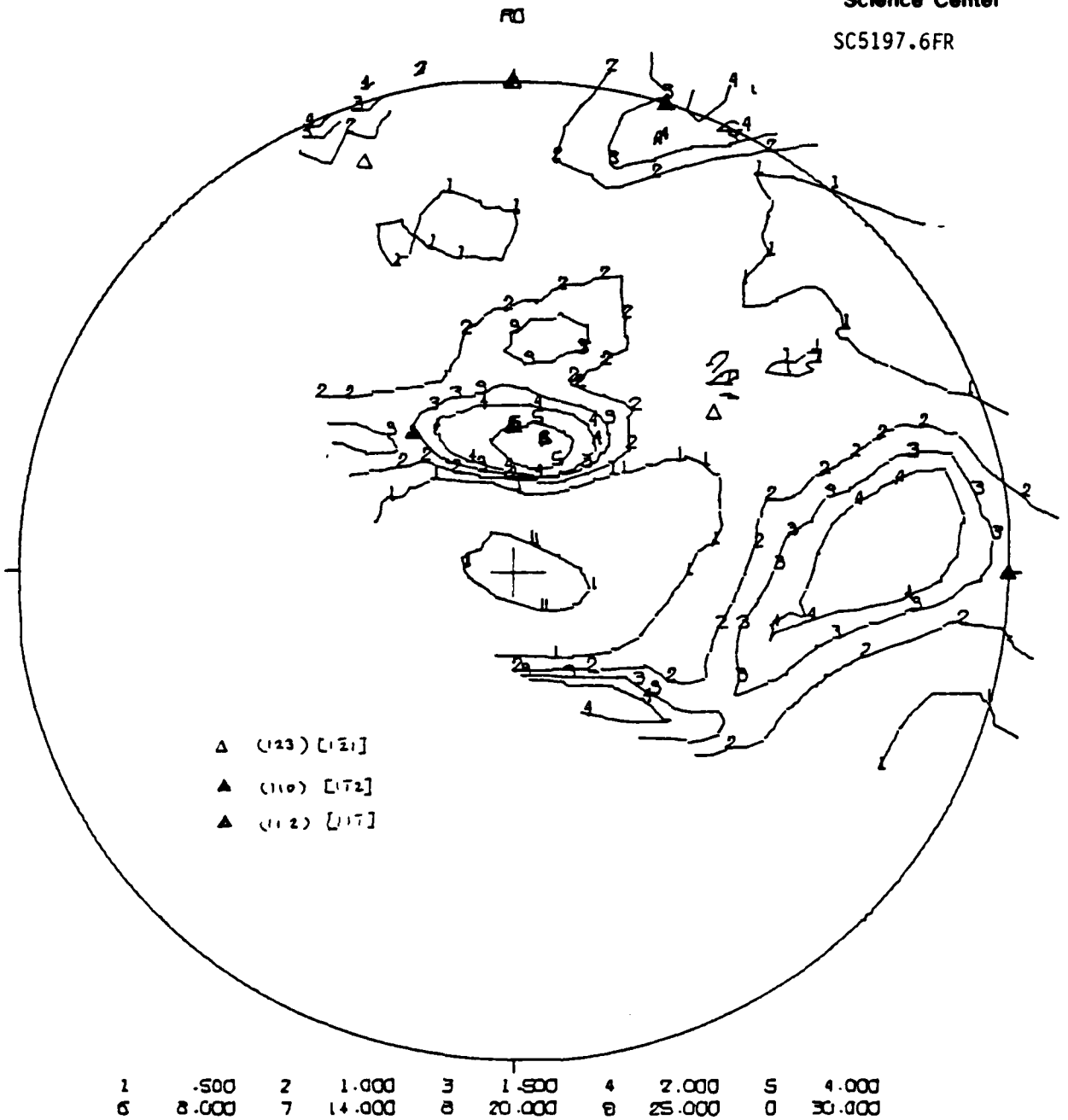

Fig. 9(a) (111) pole figure of 7039 aluminum (rolled to 0.16 in.).

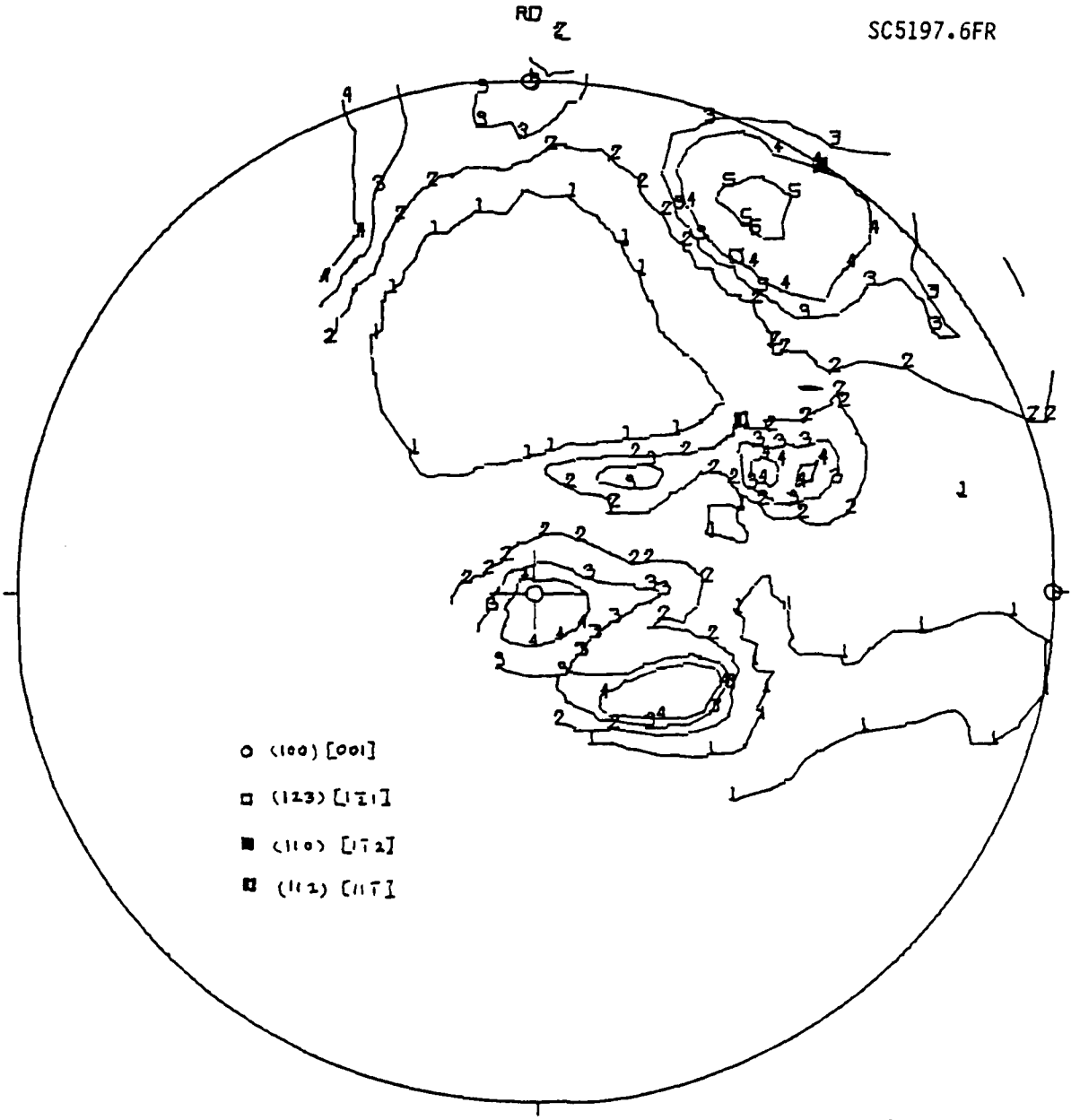

1 .500 2 1.000 3 1.500 4 2.000 5 4.000
6 8.000 7 14.000 8 20.000 9 25.000 0 30.000

BNT JOB NO.79-01871 7039-0 ALUMINUM.ROLLED DATE 05-SEP-79
RADIATION- CU AT 35KV/20MA COUNTER-PROPORTIONAL AT 2.000KV
SLITS- 2H/2V ENTRANCE, 5H/1V RECEIVING ENGINEER-DAVID G. EVANS
SCAN RATE- 1°61/MIN, 72ALPHA/MIN HKL= 200
PHA- 25V BASE, 20V WINDOW SILVER CALIBRATION
RANDOM INTENSITY (CALC) 867.7 RO=225.00 PO=-54.74

Fig. 9(b) (200) pole figure of 7039 aluminum (rolled to 0.16 in.).

indicated on the pole figures by various symbols. The surface texture of the thick plate is found to be somewhat different from that of the center. All of the samples showed some degree of cube (100) <001> texture, indicative of recrystallization. The surface has 5 times random compared to 3 times random at the center, suggesting that plate underwent fuller recrystallization at the surface. The surface also has a weak (123) $\langle 1\bar{2}1 \rangle$ type texture, which is a typical f.c.c. deformation texture. A 4 times random intensity was also observed around (113) $\langle 12\bar{1} \rangle$ pole, which is not reported normally for this material. In fact, this may simply be produced by a combination of (110) $\langle 1\bar{1}2 \rangle$ textures. The center of the 1.5 in. plate has a truer representation of f.c.c. deformation texture (110) $\langle 1\bar{1}2 \rangle$, with six times random intensity. The heavily rolled 7039 alloy is described by (123) $\langle 1\bar{2}1 \rangle$ fairly well. However, (110) $\langle 1\bar{1}2 \rangle$ components might have joined to appear as (113) $\langle 12\bar{1} \rangle$. Again, a times four random intensity is observed for the cube texture as well.

Based on Taylor factors (Figs. 2-5) several inferences may be drawn from them and pole figures. An increased cube texture component in the surface would be expected to make it more shear resistant than the center (as suggested from Fig. 4). This result has been experimentally shown to be true in the next section. Comparison for through-thickness compression resistence in this manner does not seem possible since the intensities of different deformation textures are not easily added together. However, due to strong deformation texture the plate is considered to be stronger in the through-thickness direction than in the plate plane. The plate rolled to 0.16 in. appeared to be equally effective as far as through-thickness properties are considered.

The results of the detailed orientation distribution on the Taylor factors are given in Table 2. These are calculated from the pole data (Figs. 7-9), using the computer program discussed in Section 3.0. This table indicates, as mentioned previously, that the surface region is expected to be more resistant to shear deformation due to its higher (100) <001> component. The reversal of shear and compression strength is also observed in going from the surface to the center. However, the proximity of these normalized values to unity do suggest that in all three conditions the anisotropy of plastic properties is extremely small (fracture anisotropy may, however, be present), perhaps because of the absence of strong (110) $\langle 1\bar{1}2 \rangle$ texture. It might be possible to develop such "brass type" rolling texture in aluminum either by low temperature rolling, or by alloy modification to reduce stacking fault energy, or a combination thereof. A grain refinement technique developed at Rockwell Science Center might be used to proper advantage in this regard. However, other f.c.c. materials might still offer a significant possibility of texture strengthening for ballistic purposes, as shown on A-286 steel later in this report.

Table 2

Normalized Taylor Factors (M/M_{random}) for 7039 Al

Stress-State	Angle From Rolling Direction	Surface (1.5 in. thick)	Center (1.5 in. thick)	Rolled (0.16 in. thick)
Planar Shear (through-thickness)	0°	1.04	0.949	0.983
	15°	1.04	0.955	0.983
	30°	1.046	0.955	0.989
	45°	1.046	0.9603	0.995
	60°	1.046	0.955	0.995
	75°	1.046	0.955	0.989
	90°	1.046	0.955	0.989
Compression (through-thickness)	Any	0.934	1.053	0.983

4.0 EXPERIMENTAL STUDIES ON STEEL AND ALUMINUM

The two steels included in this study were (1) 5% Ni steel, which was studied extensively in the past year, and (2) precipitation hardening, austenitic, A-286 steel. Both steels were specially rolled by Dr. Bill Hu of U. S. Steel Corporation in an attempt to develop strong textures. The 5% Ni steel was known to have strong textures to promote high strength through thickness compression and is an ideal material. The study undertaken was to examine if high temperature fabrication processes such as hot bending or welding would influence the mechanical properties of the steel. The study on A-286 steel was a new one - the object was to develop strong textures in face centered cubic steels, and study the resulting mechanical properties. The aluminum alloy used in this study is 7039 alloy, which has important armor applications. The object here was to characterize its crystallographic texture completely by pole figures, as well as to determine shear and compressive properties. The studies on each material is discussed next; starting with aluminum.

4.1 7039 Aluminum

The composition of 7039 Al is 0.24% Fe, 0.09% Cu, 0.12% Si, 2.1% Mg, 4% Zn, 0.28% Mn, 0.02% Ti and 0.12% Cr. The alloy was supplied in a naturally-aged and precipitation hardened condition by contracting officer representative, A. Zarkades of AMMRC. Grain size was somewhat large (50 μm). While this plate was 1.5 in. thick, an additional piece rolled to 0.16

in. was also supplied for examination. The x-ray pole figure data of these materials have already been reported in Section 3.1. Shear and compression results are discussed below:

Shear resistance was measured on approximately 0.100" thick strips cut at various angles (0°, 30° and 90°) to the plate rolling direction. These tests were made by pushing a rectangular tungsten carbide block through a strip held between tungsten carbide dies. For the 1.5 in. thick Al armor plate, property variation was expected between the surface and the center of the plate, and therefore, strips parallel to the surface were cut from both these areas.

Compression tests were also conducted from cylindrical samples (0.25 in. diameter, 0.5 in. tall) machined from rolling, transverse and thickness directions of the plate, respectively. The combination of shear and compression data was used to characterize the material.

The shear strength of 7039 Al armor is plotted as a function of direction (in the rolling plane) in Fig. 10. The shear strength here represents the maximum stress in the shearing operation and not shear yield stress. The surface region maintains a consistently larger strength in comparison to the center, even though the magnitude of this difference is approximately 4 ksi. According to the Taylor factors calculated in Sections 2.0 and 3.1, the greater surface shear strength is explained by a higher (100) <001> pole intensity near the surface. While the in-plane shear anisotropy is not large, the strips along the rolling direction exhibits somewhat greater strength.

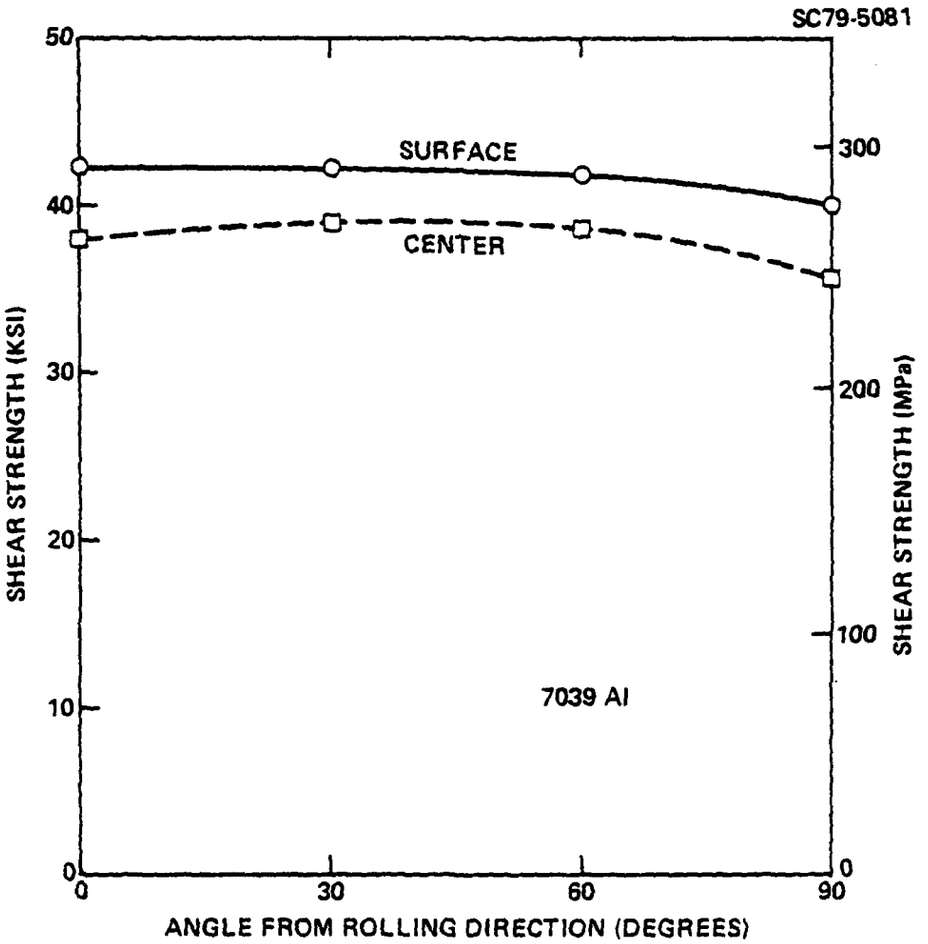

Fig. 10 Shear strength of 7039 aluminum (1.5 in. stock) as a function of rolling direction.

Teflon and mineral oil combination was used for lubrication during compression and no barreling was observed up to a strain of 0.2, thereby indicating a uniform compression test at least up to that point. True stress/true plastic strain curves for three directions in the plate are shown in Fig. 11. The compressive yield was found to lie between 55 and 60 ksi depending on the test direction. The curves show rapid initial work hardening followed by a slow approach toward a nearly steady-state stress. The specimen along the rolling direction exhibits the lowest yield and the lowest overall curve. While the yield in the thickness and transverse direction are about the same, the initial work hardening in the transverse direction is greater, thus suggesting this as the most desirable direction (nonetheless impractical) for use as armor. With increasing strain the thickness direction eventually develops slightly greater strength than transverse direction.

The larger compressive strength in the transverse direction logically fits with a smaller shear strength in that direction, as expected on the basis of anisotropy-modified von Mises yield criterion. The anisotropy observed here is not large and to a first approximation, a shear strength of nearly 40 ksi is explainable ($\sigma/2$) from a nearly saturated uniaxial stress of 80 ksi.

The influence of high strain rate deformation on 7039 aluminum has been conducted by Wulf.[14] In the strain-rate regime of 10^3-10^4/sec, the material was found to be highly rate-sensitive. While the flow stress increased with increasing strain rate, the adiabatic heating it caused led to a softening at larger strains. Deformation was highly localized in shear bands, which according to Stock and Thompson[15] experiences incipient melting. The

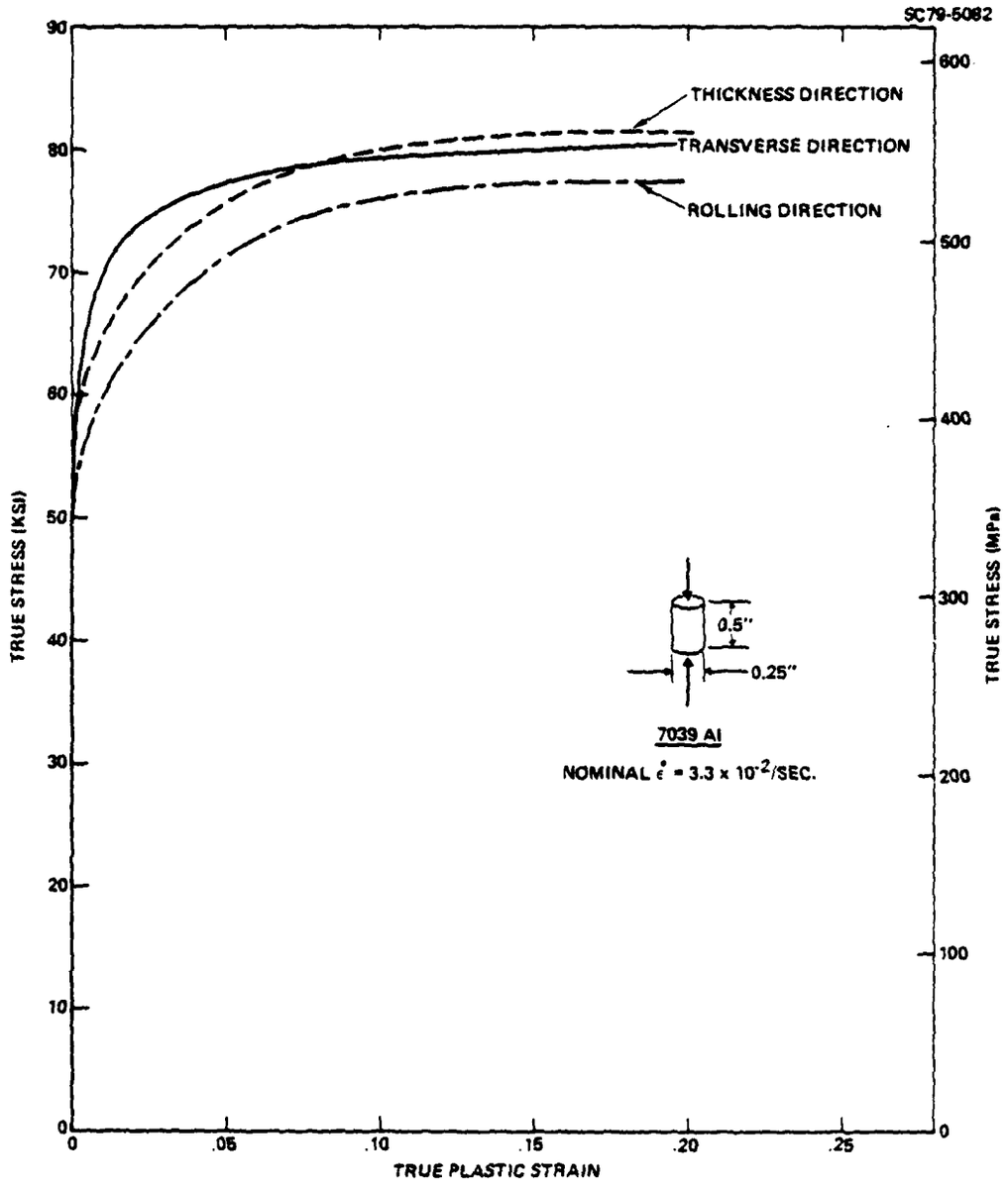

Fig. 11 Stress-strain curves in compression for 7039 aluminum.

strain-rate in the present experiment was too low to produce any such effect, however, the fact that $d\sigma/d\varepsilon$ becomes very small beyond a strain of 0.1 provides an ideal condition for strain localization into shear bands and adiabatic shear tendencies in spite of the high thermal conductivity of Al.

The sheared fracture profile is shown in Fig. 12a, which yields a shear fracture strain of approximately 2.25. However, the ballistic resistance, provided by such a high fracture strain is not extremely large since the work hardening rate is rather low. It appears that alloy modification to either increase the yield strength or increase the work hardening rate (for this yield strength) would be of value in this respect even at the expense of fracture strain. Care should be exercised, however, such that low temperature properties do not become inferior. The fracture profile also shows no unexpected effects such as delamination, which were found to occur in 5% Ni steel at ballistic velocities. Figure 12b is a fractograph from this material showing elongated dimples which are indicative of ductile fracture process. Substantial inhomogeneity was also noticed in the fracture surface possibly signifying local segregations. Since these heterogeneities were located closer to the plate center, the surface to center variation (Fig. 10) might also be related to this.

4.2 5%-Ni Alloy Steel

Motivated by the improved ballistic performance with increasing (111) + (112) intensity in the 5% Ni steel plates, a plate was further rolled to a thickness of 0.25 in., to yield a (111) intensity in the plate 11 times

SC80-10146

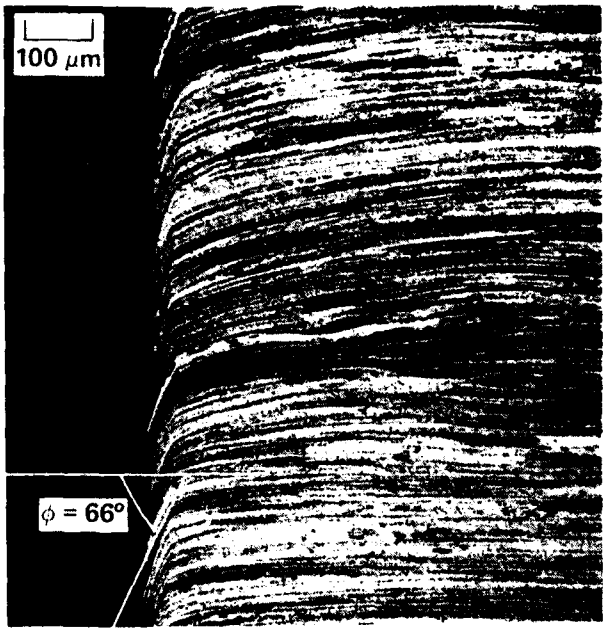

(a)

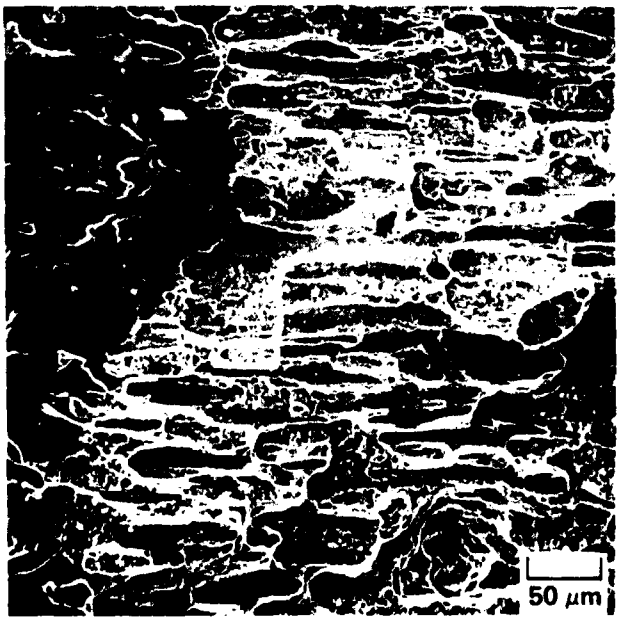

(b)

Fig. 12 (a) Shear fracture edge and (b) fracture surface for 7039 aluminum.

random. Shear and tensile tests were carried out on this material as well as two of the 0.5 in. plates from a previous study.[1] Their mechanical properties are listed in Table 3 next to their texture intensities.

Table 3

Mechanical Properties of 5% Ni Steel

Texture Intensity (Thickness)	Yield Strength (ksi)	Tensile Strength (ksi)	Max Shear (Ksi)	Total Elongation
3.8xR(1/2 in.)	230	293.8	189.2	9%
9.1xR(1/2 in.)	260	301.2	195	6%
11xR(1/4 in.)	251.5	297.6	178	7.5%

It is observed that total elongation increased and strength decreased with increase in texture intensity from 9 to 11. The strength decrease is evident in both tension and shear tests and may be responsible for the poorer ballistic properties of the 1/4 in. rolled steel. A further microstructural degradation has been observed in the 1/4 in. rolled plates. Figure 13 shows cross-section of sheared test specimens indicating substantial fiber bending at the tear location. However, the layers are filled with inclusions and second phase materials, which tend to join and cause delamination. This has also been observed in these tests.

Warm fabrication treatment was simulated on the 5% Ni martensitic steel (hot rolled and quenched) of Hu et al.,[3] which was used in last year's research program. The simulation amounted to exposures of strips (.080"

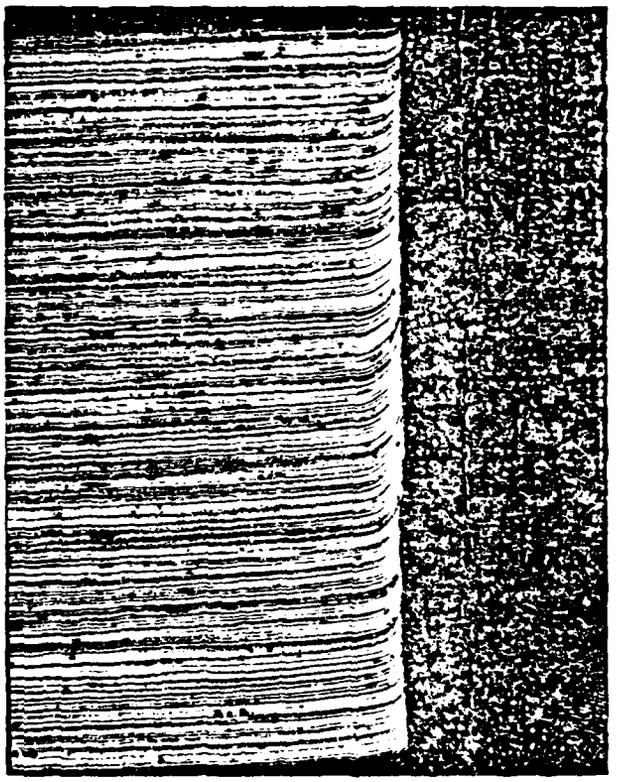

Fig. 13 A 50X photomicrograph of 1/4" rolled 5% Ni steel near sheared edge showing second phase in the banded structure.

thick) cut from the plate rolling direction at 621°C (1150°F) and 677°C (1250°F) for 1/2 hour in vacuum environment, followed by air cooling. The strips were wrapped in Ta foil to minimize oxidation. Both the weakest and strongest texture intensities I_{max} = 3.8 x and 9.0 x random) were treated in this manner. Subsequent to the thermal treatment tensile specimens were ground from some of the strips and both tensile and shear tests were conducted.

The results of vacuum annealing heat treatment on the 5% Ni steel armor are shown in Table 4 and are expected to indicate roughly the influence of a warm fabrication process. Actual fabrication would take shorter time than 1/2 hour, however, heat up time might be longer. The defect structures introduced during warm fabrication would produce increased strength and toughness in comparison to the values listed in Table 4. With such expected differences in mind, the maximum strength in shear is found to drop approximately 22% by annealing at 621°C and nearly 25% for the 677°C treatment. The difference between the high and low texture intensity was small. Tensile yield drop is also about 25% for the intense textured steel (I_{max} = 9.81) at 621°C but considerably more (nearly 70%) at 677°C. The lower texture intensity material also showed a drop to 15% at 621°C and 63% at 677°C. This 56°C increased in temperature appears to be quite dramatic in reducing the tensile strength even though the shear strength is not altered significantly. A partial reason for this might lie in the increased tensile ductility as reflected by the total elongation values. While such large strength reductions may not occur during the processing step, a 15% strength loss may be expected on account of warm processing of the quenched 5% Ni armor steel plate.

Table 4

Shear and Tensile Properties of Steel Armor
Before and After Annealing Heat Treatment

Parameter Measured	Texture Intensity (x Random)	Strength (ksi)* for the Condition		
		As-Received	621°C/30 min	677°C/30 min
Shear Strength (max)	3.8	189.2	151.0	142.4
	9.1	195.0	148.4	145.5
Tensile Yield Strength	3.8	230	195.9	84.6
	9.1	260	194.5	77.4
Tensile Elongation	3.8	9%	12%	15%
	9.1	6%	11%	14%

*Values averaged from three tests.

4.3 A-286 Steel

This is a heat resistant precipitation hardenable Fe-Ni-Cr-Mo alloy of the following nominal composition:

Table 5

Composition of Wrought A-286 Steel (wt %)

C	Mn	Si	Cr	Ni	Mo	Ti	Al	V	Fe
0.008	1.35	0.5	15	26	1.25	2.0	0.25	0.3	Remainder

In the precipitation hardened condition this steel offers excellent combination of strength and toughness. This steel is weldable and has been used in gas turbine and other creep-resistant applications. While good

ballistic performance is expected of this material in its conventionally processed condition, it was felt that appropriate thermochemical processing can generate additional texture strengthening. Since this is an austenite-stabilized steel, guidance was available from Kula and Lopata's[16] work on 4340 steel, which was rolled in the austenitic (γ) state. In their work it was estimated that a strong texture developed in γ which upon quenching gave rise to a strong $(110)_\alpha$ texture through Kurdjumov and Sachs transformation. This suggested that in A-286 steel, a possibility exists for developing a strong $(111)_\alpha$ deformation texture, which according to Fig. 3 suggests superior performance.

Eight coupons of A-286 (1.5 in. x 4 in. x 0.075 in.) processed by different thermomechanical treatments, were supplied by Dr. Bill Hu of U.S. Steel Corporation. These strips were first solution-treated at 1800°F and then rolled (90%) at 1800°F, 1500°F, 900°F and 80°F respectively. One batch of four coupons were supplied in this as-rolled state. The other batch of four underwent recrystallization at 2000°F and quenched. The U.S. Steel designations of these specimens are summarized in Table 6, and a description of their pole figure (courtesy Bill Hu) follows.

P941-X7: Very weak, intensity maxima about 3
-X5: Very strong, Copper-type, intensity maxima 8.
-X2: Very strong, Copper-type but broadened, intensity maxima 8.
-X2: Strong, Brass-type, intensity maxima 6.

P941-X7R: Practically random.
-X5R: Mainly (111) <110> plus (001) <110>, intensity maxima about 5.

-X2R: Mainly (112) <111>, intensity maxima about 7.

-X8R: Mainly (110) <112> plus (110) <001> (in situ recrist.), intensity maxima about 5.

(Copper-type, mainly (110) <112>, (112) <111>, plus (123) <412>; Brass-type, mainly (110) <112> plus (110) <001>.)

Table 6

Thermomechanical Treatments* of A-286 Steel

Rolled		Rolled and Recrystallized		
Designation	Rolling Temperature	Designation	Rolling Temperature	Recrystallization Temperature
P941-X7	1800°F	P941-X7R	1800°F	2000°F
P941-X5	1500°F	P941-X5R	1500°F	2000°F
P941-X2	900°F	P951-X2R	900°F	2000°F
P941-X8	80°F (CR)	P941-X8R	80°F (CR)	2000°F

*All materials were first solution treated at 1800°F for 1 hour.

Microstructures of two of these steels are shown in Fig. 14. The rolled structure is banded with fine precipitates observable. The recrystallized structure shows equiaxed grain structure 50 μm diameter on the average. It is speculated that some amounts of grain growth also occurred during the recrystallization treatment.

The tensile stress-strain curves in the recrystallized condition are shown in Fig. 15. While these data are essentially independent of rolling temperature, rolling at 900° and 1500°F appear to provide slightly improved strength. The tensile yielding is found to occur around 33 ksi in the

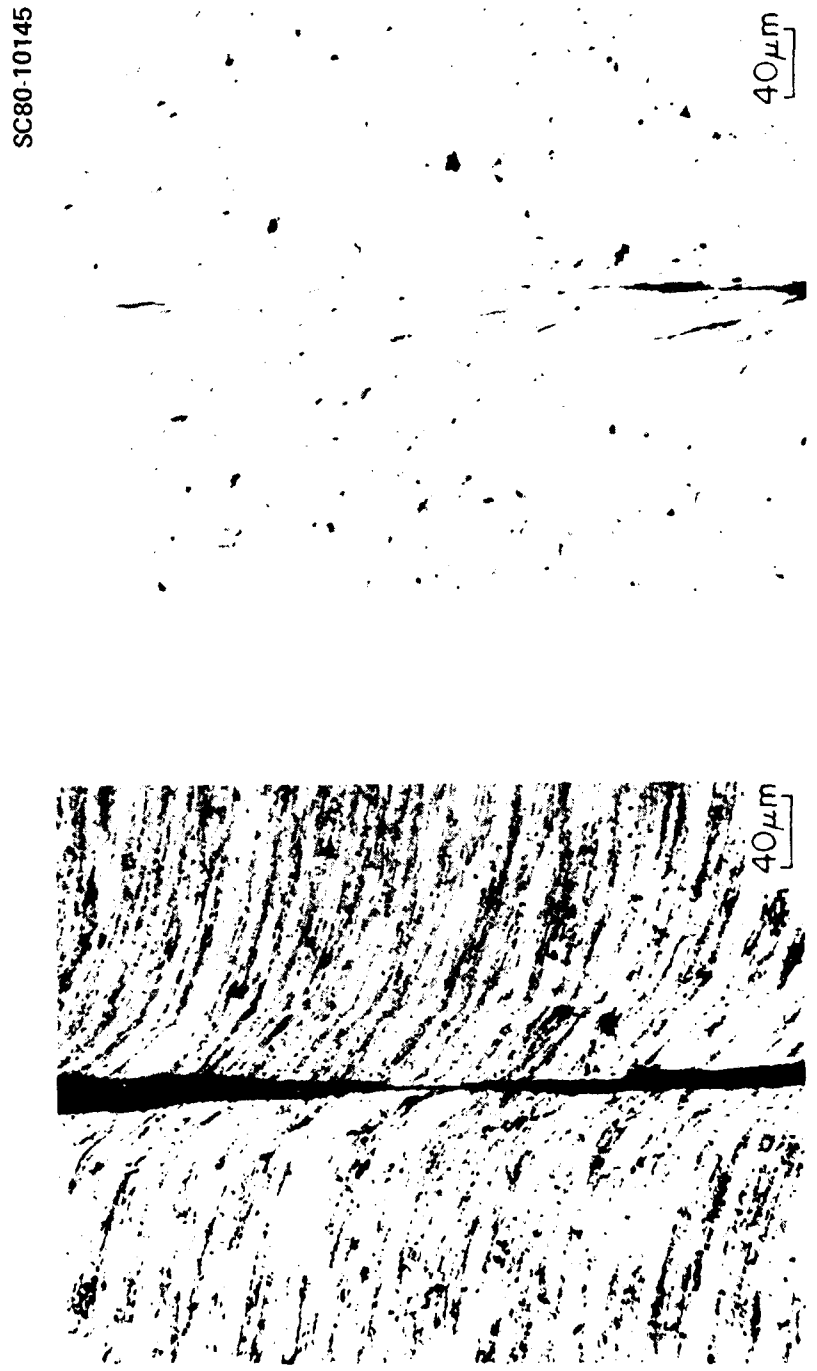

Fig. 14 Micrographs of A-286 steel in two different conditions of thermal treatment.

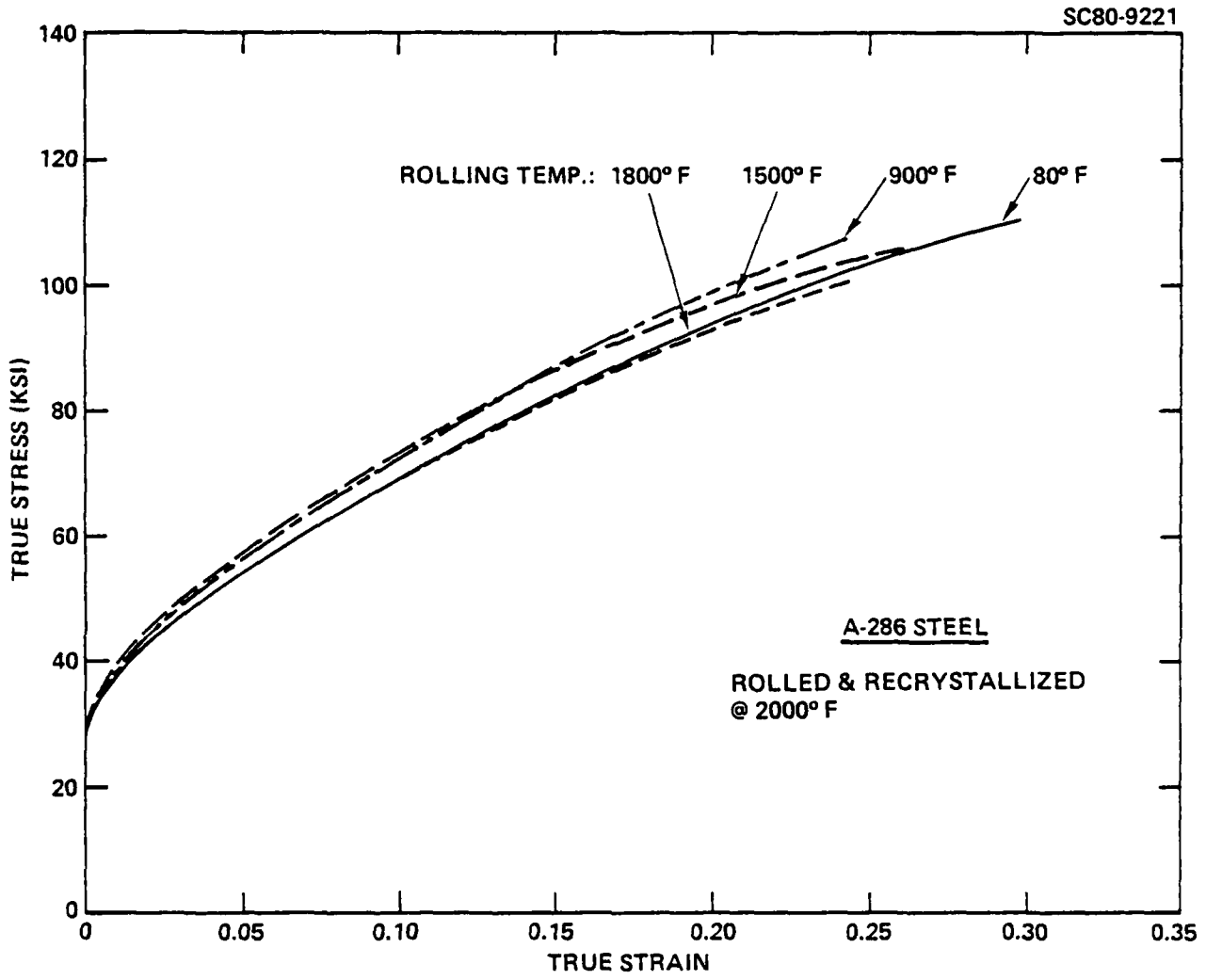

Fig. 15 Tensile stress/strain data for A286 steel after rolling and recrystallization.

recrystallized state, similar to a mild steel. Work hardening is quite pronounced and substantial elongations are possible (see Table 7).

Table 7

Tensile Properties of A-286 Steel

Condition	I.D.	Yield Stress (ksi)	Ultimate Tensile Stress (ksi)	Uniform Elongation (%)	Total * Elongation (%)
Rolled	X7-HR	36	84.6	30	44
	X5-HR	95	125	11	17
	X2-HR	96	164	1.5	5
	X8-HR	100	162	1.3	5
Recrystallized	X7-R	30	79.3	32	38
	X5-R	31.2	80.7	31.5	42
	X2-R	31.2	80.7	31.5	42
	X8-R	32	81.4	31	36

*Elongation measured over 1 in. gage length.

The rolled material (Fig. 16) on the other hand, exhibited increasing strength with decreasing rolling temperature. Rolling at 1800°F generates strength properties somewhat better (37 ksi) than the recrystallized material, while 1500°F rolling causes significant improvement (approximately 95 ksi). The lower rolling temperatures (900°F and 80°F) produce extremely high strength (~ 160 ksi), possibly due to high dislocation density. This is speculated on the basis of the fact that the rolling at 80°F is no different for such high strength material from that at 900°F. The ductility drops, however, with decreasing rolling temperature and these are listed in Table 7.

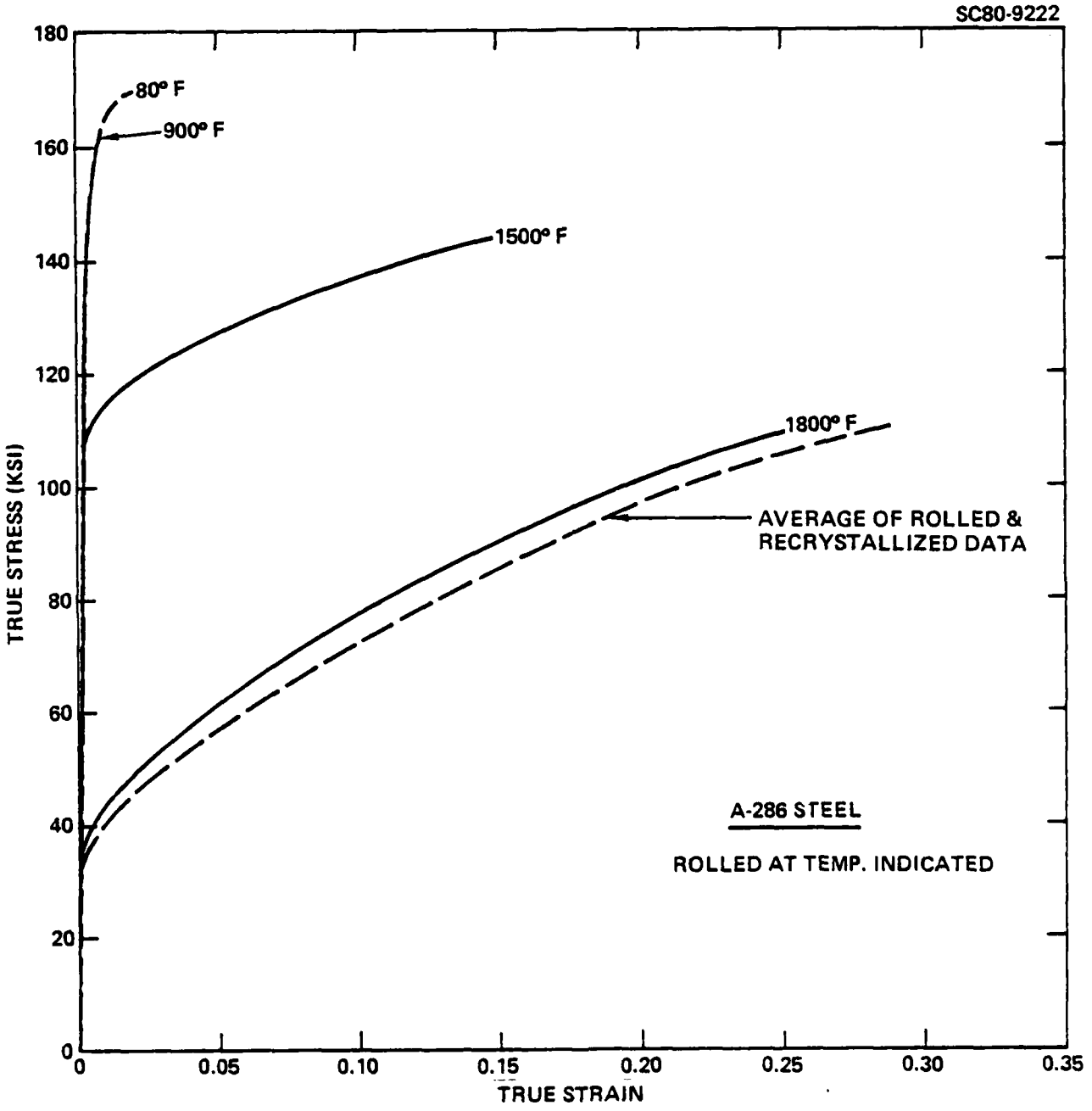

Fig. 16 Tensile stress/strain data for rolled A-286 steel compared against that for recyrstallization material.

The limited supply of the A-286 steel did not permit a detailed investigation of its properties in various directions in the plate (particularly after cropping off the shear cracked edges). In addition to the tensile tests on the as-rolled and as-recrystallized materials described above, rectangular shear test specimens (0.5 in. x 3 in.) were machined for studies in both aged and as-received condition. Furthermore at least five small pieces (a 5 in. x 0.5 in. or smaller) of the same material were stacked together and bonded with epoxy to produce a 0.4 in. thick plate. Through-thickness compression test specimens (0.25 in. diameter) were machined from these five layer plates and aged at 1300°F for 8 hours for precipitation hardening before testing. Half of the shear test specimens were also aged under the same condition before testing.

All shear test data are plotted in Figs. 17(a) and (b) as a function of rolling temperature. Shear yield strength values are indicated by dashed curves while the maximum strength in shear is indicated by solid curves. Figure 17(a) shows a large spread between the yield and maximum strength values for the recrystallized material, as observed in the tensile data. The shear yield strength values are roughly half of the corresponding tensile values in both rolled and recrystallized conditions. The rolling temperature effects on the rolled data is very similar to the tensile test results, an increase in temperature bringing closer to the recrystallized values.

The two lowest rolling temperatures (80°F and 900°F) appear to be the most promising from the standpoint of texture strengthening since they contain strong "brass-type" textures or (110) and (112) textures (see Fig. 3). This

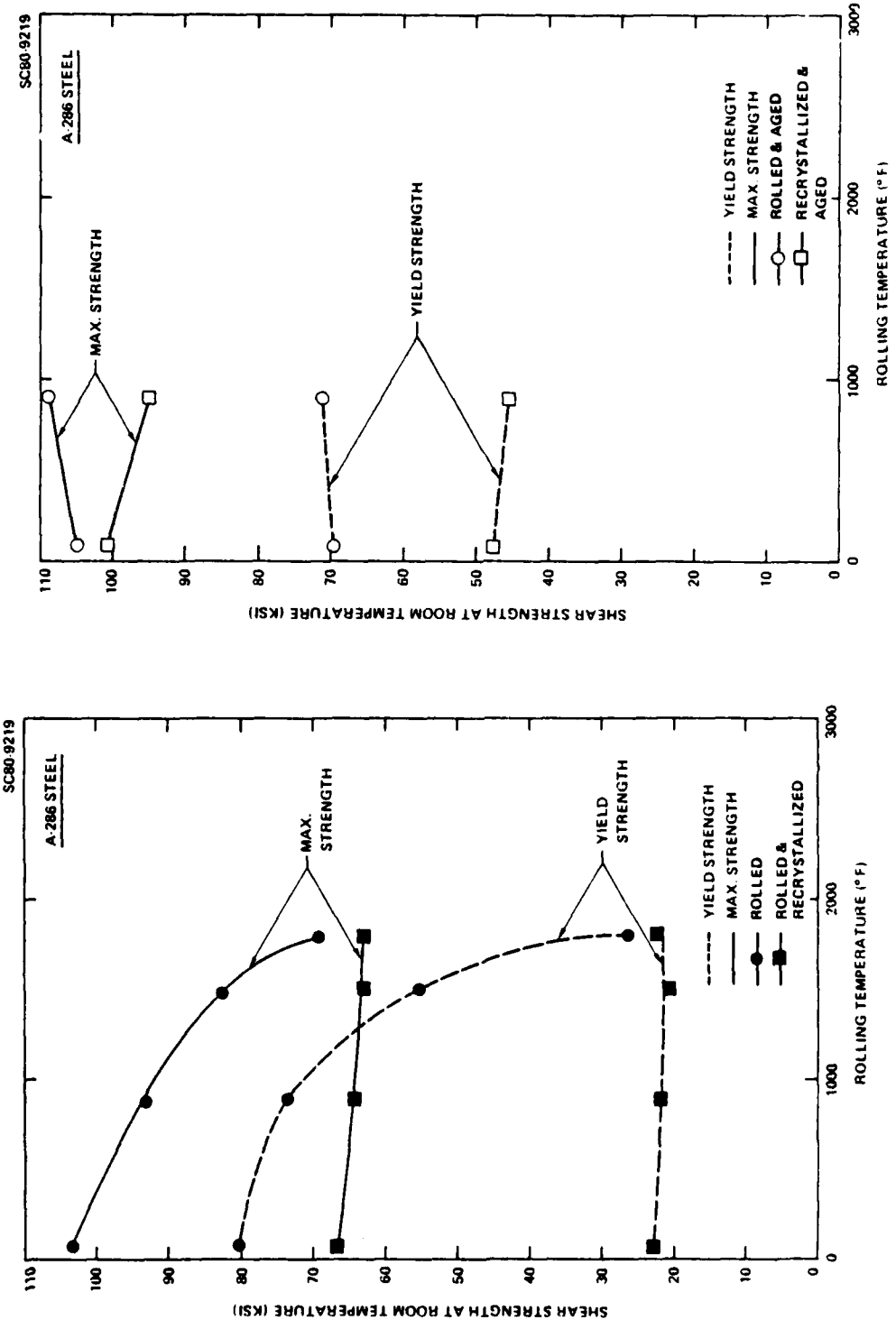

Fig. 17 Shear test results as a function of rolling temperature for A-286 steel (a) before and (b) after aging treatment.

is why these two materials were used in further age hardening studies. Figure 17(b) shows yield and maximum shear strength values of these materials. Significant strength improvements are observed as a result of precipitation hardening. While the maximum shear strengths for rolled and recrystallized materials now approach each other, the yield strength for the rolled material is still higher due to the higher dislocation density. Aged X2 material (rolled at 900°F) appears to have the highest shear strength perhaps because of its retention of copper type texture throughout precipitation.

The compression test results on the five layer specimens is shown in Fig. 18. Work hardening is significant in the recrystallized and aged materials and quite respectable in the rolled and aged material. As far a yield strength level is concerned, the compression data are similar to the shear data. However, the degree of change is different under different conditions of treatment. A measure of plastic anisotropy may be obtained from comparing yield strengths in compression and shear. The resulting R values (anisotropy parameter) calculated from the following equation:

$$\frac{\sigma_{comp}}{\sigma_{shear}} = \sqrt{1 + 2R} \qquad (11)$$

are listed in Table 8. While these values are strictly applicable to yield strength level and would approach unity with increasing plastic deformation, nevertheless the extremely high R estimated for the rolled and aged steels are extremely encouraging from the standpoint of ballistic resistance. The high through-thickness strength levels of 190 ksi (or over) also suggest that

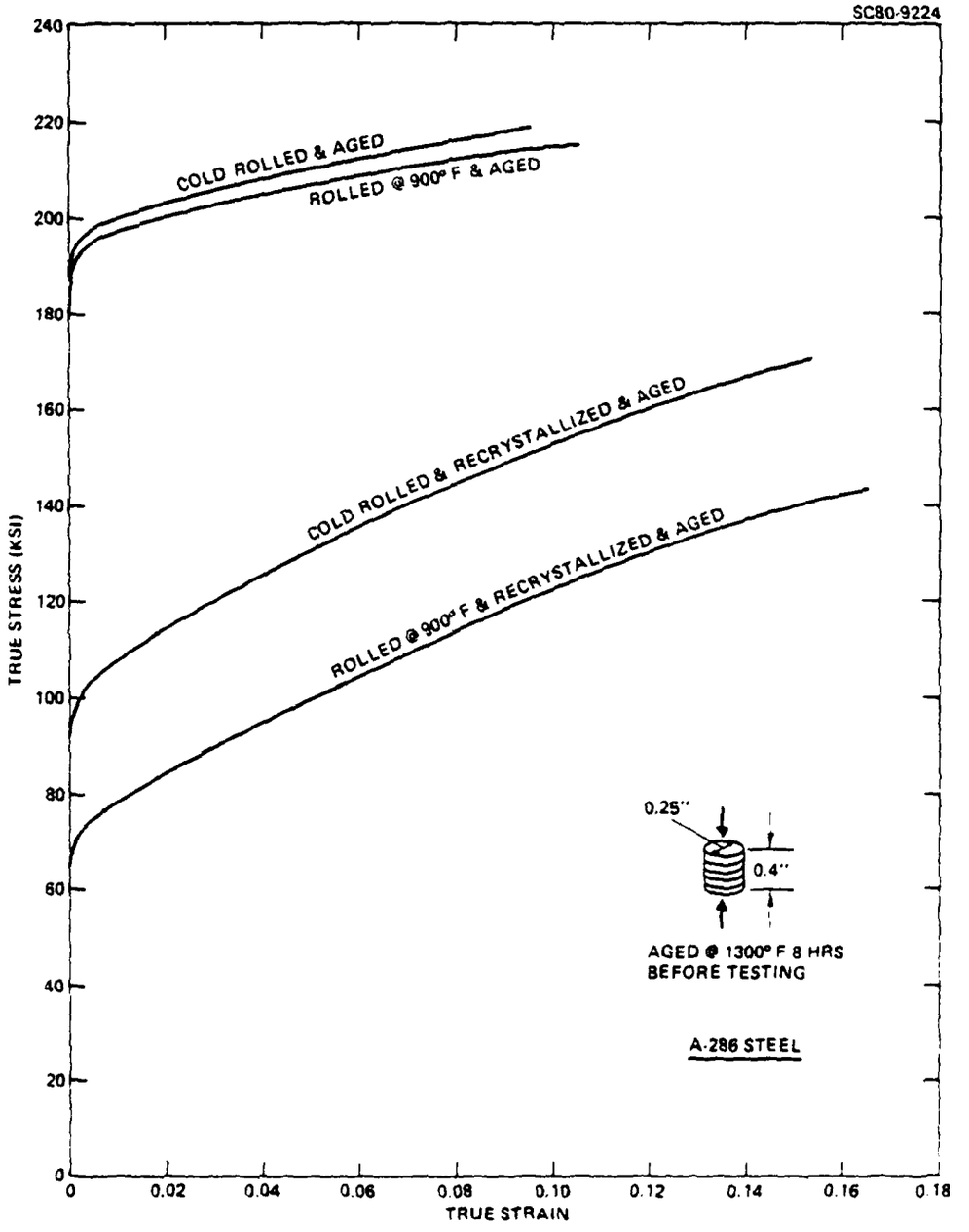

Fig. 18 Through-thickness compression test results of rolled and recrystallized A-286 steel, after aging treatment.

this is a good possibility. However, these strength values are somewhat less than those of 5% Ni Steel, and it is doubtful if further improvement of ballistic properties over this material is likely. It is suggested, however, that future studies should aim at the ballistic testing of this material.

Table 8

Strength Anisotropy of A-286 Steel

Condition	Yield Strength (ksi) (Shear)	Yield Strength (ksi) (Compression)	Estimated R
Rolled at 80°F (X8) + Aged	70	195	3.38
Rolled at 900°F (X2) + Aged	71.5	192	3.10
X8 + Recrystallized + Aged	47.5	100	1.72
X2 + Recrystallized + Aged	46	71	0.69

4.4 Measurement of Young's Moduli

Prompted by the observed relationship between elastic modulus anisotropy and the anisotropy of plastic properties, a study was undertaken to measure Young's modulus of a number of test materials in a variety of processing conditions.

Measurement of Young's modulus was carried out on 5% Ni steel and 7039 aluminum armor materials, both in as-received as well as rolled condition. The modulus measurement was carried out by an ultrasonic pulse echo

technique with a 15 MHz transducer. The average time delay between successive pulses was measured to obtain the velocity of longitudinal elastic wave. Specimen density was determined separately from mass and volume measurements. Young's Modulus, E, was calculated by using the equation:

$$E = \rho c_L^2 \frac{(1 - 2\nu)(1 + \nu)}{(1 - \nu)}$$

where ρ = density, c_L = velocity of longitudinal wave, ν = Poisson's ratio. The Poisson's ratio for steel was chosen to be 0.26 and for aluminum 0.33 from the handbook.

Young's modulus was measured from three orthogonal directions of 0.5 in. cube specimens of as-received materials. For the 1/4 in. rolled stel and 0.16 in. rolled 7039 aluminum measurements were possible only in the thickness direction. These measurements are tabulated below (Table 9).

A small increase in elastic modulus is recorded in going from I_{max} = 3.8 to I_{max} = 9.1. The work of Stickels and Mould[17] has shown that such a small change in Young's Modulus can mean a significant increase in normal plastic anisotropy (R). This, in turn, would be responsible for the high through-thickness compression resistance of the steel of I_{max} = 9.1. In the case of 7039 aluminum, the elastic anisotropy is essentially nonexistent.

Table 9

Young's Moduli

Material	Test Direction	Young's Modulus	Texture Intensity
5% Ni Steel (0.5 in. thick)	Rolling	30.56	
	Transverse	31.09	3.8
	Thickness	30.62	
5% Ni Steel (0.5 in. thick)	Rolling	30.62	
	Transverse	31.25	9.1
	Thickness	31.86	
Rolled 5% Ni Steel (1/4 in. thick)	Thickness	31.69	11.0
7039 Al (1.5 in. thick)	Rolling	10.79	
	Transverse	10.72	--
	Thickness	10.79	
7039 Al (0.16 in. thick)	Thickness	10.72	--

5.0 BALLISTIC LIMIT CALCULATION FOR FLAT-ENDED PROJECTILE IMPACT

Plate penetration by projectile impact is an extremely complex problem for analysis, particularly when plastic work of deformation has to be accounted for in addition to the propagation of elastic waves in the solid. Consideration of certain aspects of these effects are observed in the literature.[17-20] The work of Recht and Ipson[10] primarily considers momentum transfer and plug acceleration for developing the conditions of plug ejection by shear. Woodward and de Morton[18] have considered strain hardening properties of plate material as well as plug acceleration and the ballistic wave propagation in their velocity/stress relationships. However, heat generation and strain-rate sensitivity of flow stress have not been taken into account. Furthermore, the influence of plastic anisotropy (due to crystallographic texture) of plates resulting from thermomechanical processing effects have not been considered either.

The purpose of this work is to emphasize the internal plastic work performed on the plate material whose strain hardening, strain-rate sensitivity and plastic anisotropy properties are included in the calculation of plastic work. Furthermore, the deformation work is not simply restricted to shear plugging type action, but a combination of through-thickness compression and shear on planes of velocity discontinuity (as in the upper bound approach). The heat generation is taken into account and in an approximate manner the heat conduction away from the deforming zone has also been incorporated in the calculation. The interest here is in the prediction of

ballistic limit, and while it is realized that wave propagation effects become increasingly important at extremely high projectile velocity, it is assumed that this is not a significant factor in the perforation of at least up to 0.5 in. (12.7 mm) thick steel plates as long as the work for plug acceleration is taken into account. Furthermore, the deformation (mushrooming) effect of the projectile is neglected in the analysis.

The analytical scheme followed here involves division of the plate into a number[50] of small elements in the through-thickness direction (Fig. 19). Upon projectile impact, firm contact with the plate is assumed to occur immediately, as the plug accelerates to a velocity which is common to the plug and the penetrator. This simple, kinetic energy balance is given by,

$$1/2\ M_p\ v_o^2 = 1/2(M_1 + M_p)\ v^2 \qquad (12)$$

where M_p = projectile mass, M_1 = plug mass, v_o = impact velocity, and v = common velocity after the energy transfer. (When plug dimensions are known, this velocity can be determined). Attainment of this velocity is a prerequisite for the plastic penetration process to begin at such a high rate of impact.

Plastic deformation is supposed to begin by through-thickness compression of the elements underneath the penetrator. In the case of a plane strain problem, slip line fields can be constructed for the penetrator entry by extrusion of material upward (along the sides), as shown in Fig. 20. This is generally the situation when the plate is entirely supported from the

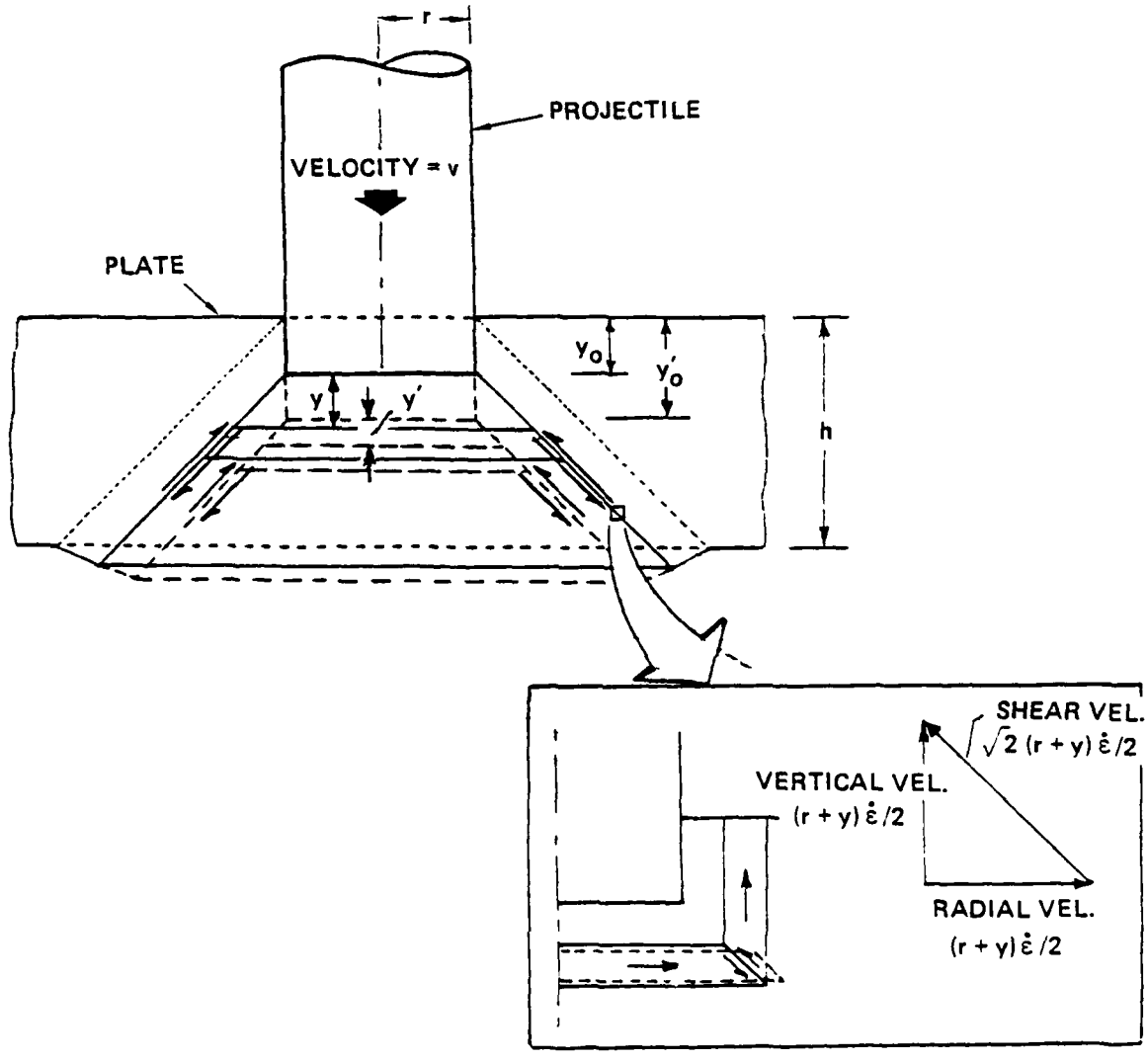

Fig. 19 Schematic of the shear-based ballistic perforation process and velocity hodograph (insert).

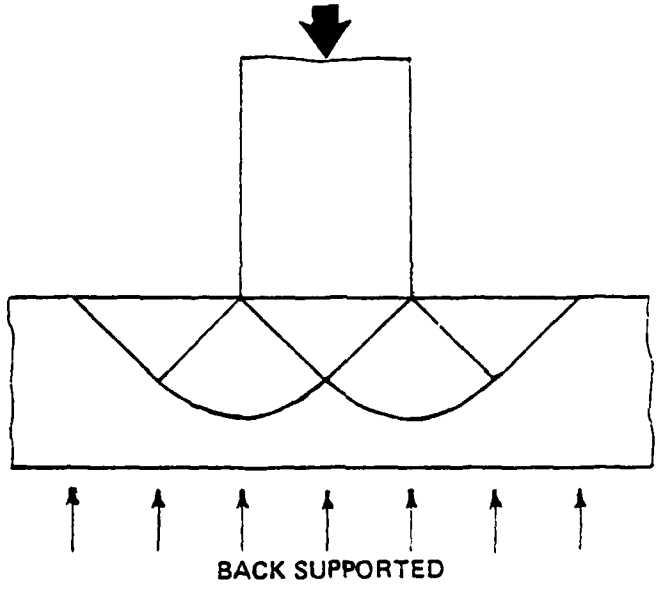

Fig. 20 Slip line fields for plane strain indentation problem.

back. In the case of an axisymmetric projectile with no back plane support for the plate (Fig. 19), however, the planes of velocity discontinuity must allow plate bending across a boundary of shear.

Thus, the boundary of the elements undergoing compression is defined by a 45° shear cone emanating from the bottom end of the projectile at all times during the perforation process. The compressive strain in each element is assumed to be the same everywhere, varying from one element to the next. The compressive action in each slab element pushes material outward, which then suffers a shear displacement at the boundary. This causes a relative upward displacement of the excess material with respect to the slab itself (Fig. 19, inset).

In the case of very thick plates, upward extrusion of part of this excess material might be significant, however, it is assumed here that the relative displacement leads only to the downward motion of the slab by an amount necessary to move the excess material above the shear plane.*

The plug, defined by the truncated shear cone, at the initial instant of impact has a mass, M_1, given by

$$M_1 = \pi \left\{ \frac{r + (r + h)}{2} \right\}^2 h\rho \qquad (13)$$

*For plate thicknesses no more than twice the projectile diameter, no upward extrusion on the top surface of the plate has been observed.[21]

where, r = penetrator radius, h = initial plate thickness and ρ = density of plate material. When this value of M_1 is substituted in Eq. (12), the common velocity, v, to which the plug is accelerated is obtained. This also constitutes a slowing of the projectile.

Plastic perforation process can now begin under kinetic energy supplied by the remaining velocity of the projectile. If y_0 is the perforated thickness at an instant when y is the distance of an element from the bottom of the projectile, and if after a time Δt, these dimensions become y_0' and y', respectively, then the volume of material leaving the element in question (during this time increment) is

$$\Delta V = \pi h_0 \left[(r + y)^2 e^{-\varepsilon} - (r + y')^2 e^{-(\varepsilon+\Delta\varepsilon)}\right] \qquad (14)$$

where h_0 = initial element thickness, r = projectile radius, ε and $\varepsilon + \Delta\varepsilon$ = compressive strain in the element before and after the time increment, respectively. This volume of material would add to a vertical cylinder of average radius, $r + (y + y')/2$, and average wall thickness, $h_0 \left\{ e^{-\varepsilon} + e^{-(\varepsilon+\Delta\varepsilon)} \right\}/2$, whose length increases by an amount, Δy, the vertical component of the relative shear displacement, where

$$\Delta y = (y_0' + y') - (y_0 + y) \qquad (15)$$

Thus the volume gained in the cylinder is

$$\Delta V = 2\pi\left(r + \frac{y + y'}{2}\right) h_0 \left\{\frac{e^{-\varepsilon} + e^{-(\varepsilon+\Delta\varepsilon)}}{2}\right\}\Delta y \qquad (16)$$

which must equal to the expression in Eq. (14). Now, if v is the projectile velocity during time increment Δt, $y_0' - y_0 = v\Delta t$. This can be substituted in Eq. (14) and subsequently equating Eqs. (14) and (16), we obtain

$$v\Delta t = \frac{(r + y)^2 - (r + y')^2 e^{-\Delta\varepsilon}}{(r + \frac{y+y'}{2})\{1 + e^{-\Delta\varepsilon}\}} + (y - y') \qquad (17)$$

The perforation problem may be solved by assuming the process to be quasistatic in small time increments, during each of which the projectile velocity, v, is constant. Starting from the first element ($y = y' = 0$), the resulting strain increments are calculated to statisfy Eq. (18). Once the strain in a given element is known, the new position, y', for the next element can be obtained by summing the preceding element thicknesses.

To determine the internal plastic work done during perforation, the following stress-strain-strain-rate relationship is used:

$$\sigma = K\varepsilon^n + L\dot{\varepsilon}^m \qquad (18)$$

where σ = stress, ε = strain, $\dot{\varepsilon}$ = strain rate, K = strength constant, n = strain hardening exponent and m = strain-rate sensitivity. This additive constitutive law is applicable reasonably well to high strain-rate deformation

as evidenced by stress-strain curves at various strain-rates that are nearly parallel to one another.[22] This kind of data has been developed for mild steel and high strength steel, and high hardness armor is not believed to behave significantly differently. In other descriptions of constitutive law the rate-sensitive part of the stress is given by $M_1 \log (\dot{\varepsilon}/\dot{\varepsilon}_0)$ where M_1 is the rate sensitivity parameter and $\dot{\varepsilon}_0$ is a reference strain rate at which the second term is vanishingly small. However, it is not clear if this description offers any greater accuracy over Eq. (18).

The computation of plastic work rate in each element requires summing the work rate in compression with that in shear. The velocity hodograph illustrated in Fig. 19 (inset) suggests that the shear velocity is $\sqrt{2}(r + y)\dot{\varepsilon}/2$. Since the truncated conical surface area for shear is $2\sqrt{2\pi}(r + y)\, h_0\, e^{-\varepsilon}$, and the elemental volume undergoing compression is $\pi(r + y)^2\, h_0\, e^{-\varepsilon}$, the plastic work increment in each element is:

$$\dot{w}_p = \sigma \cdot \dot{\varepsilon} \cdot (\text{volume}) + \tau \cdot (\text{velocity}) \cdot (\text{surface area})$$

$$= \sigma\dot{\varepsilon}\, \pi(r - y)^2\, h_0\, e^{-\varepsilon} + \tau \sqrt{2}\, (r + y)\, \frac{\dot{\varepsilon}}{2}\, 2\sqrt{2\pi}(r + y)\, h_0\, e^{-\varepsilon} \tag{19}$$

Assuming roughly that $\tau = \sigma/2$, the plastic work increment rate can be written as

$$\dot{w}_p = 2\sigma\dot{\varepsilon}\, \pi(r + y)^2\, h_0\, e^{-\varepsilon} \tag{20}$$

In reality, since strain rate at the shear boundary is much greater than the strain rate within the element, $\tau > \sigma/2$, thus $\dot{w}_p$ in Eq. (20) is an underestimate. The total plastic work rate, $\dot{W}_p$, is obtained by summing these rates for all elements.

The frictional work on the projectile bottom is neglected, however that on the projectile cylindrical surface is calculated according to the scheme shown in Fig. 21. Since normal pressure is nearly σ at the bottom end, the average frictional force, F, is $(\mu\sigma/2)\ 2\pi r y_o$, which leads to a work increment rate

$$\dot{W}_f = \pi\mu\sigma r y_o v \tag{21}$$

where μ = coefficient of coulomb friction. A lower bound value of the total work increment rate, $\dot{W} = \dot{W}_p + \dot{W}_f$, is obtained after substituting σ from Eq. (18).

Now if the projectile is assumed to have a velocity is v during a small time increment, Δt, its kinetic energy at the end of Δt is

$$\frac{1}{2} M_p v'^2 = \frac{1}{2} M_p V^2 - \dot{W}\,\Delta t \tag{22}$$

where v' = velocity at the end of the time increment. The latter is thus given by,

$$v' = \sqrt{v^2 - \frac{2\dot{W}\Delta t}{M_p}} \tag{23}$$

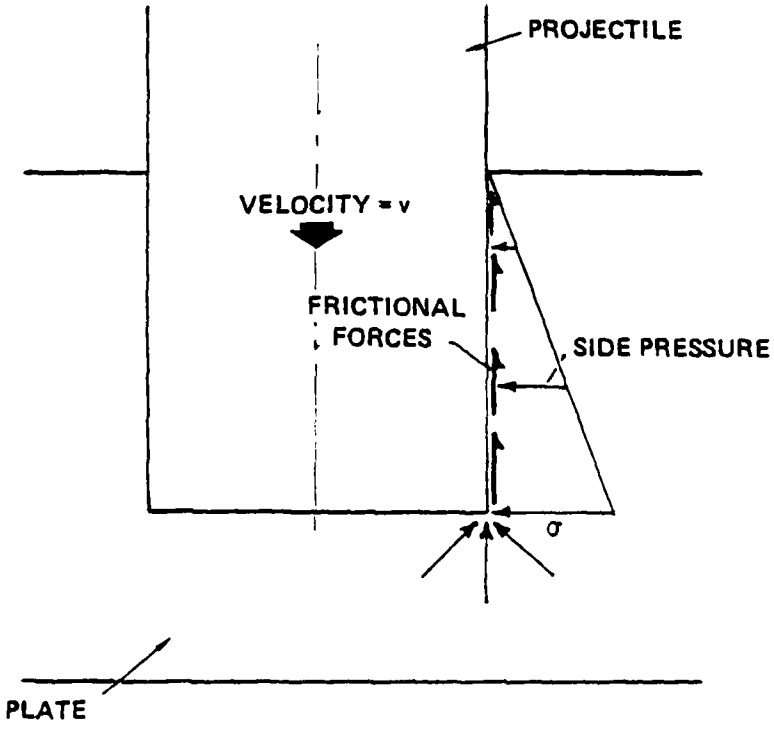

Fig. 21 Approximate pressure distribution and friction forces on the side surface of projectile.

which progressively decreases with time. The perforation process is thus simulated by allowing the projectile to move stepwise into the plate and reestablishing the shear boundary locations as indicated in Fig. 19. The overall deformation zone shrinks during this process thus leading to progressive bulging on the back of the plate (see Fig. 19). After the projectile has penetrated sufficiently, if shear fracture were to occur on these boundaries, a plug with shear ledge will be ejected. (No back spalling or shattering failure is simulated by this model).

The influence of plastic anisotropy of plates resulting from preferred crystallographic orientation is simply accounted for through the normal anisotropy parameter, R, with the assumption that the plate is isotropic in its plane.[23] Under this assumption the through-thickness compressive stress (σ_t) in the terms of in-plane stress (σ) is given by the relationship:

$$\sigma_t = \sqrt{\frac{1 + R}{2}}\,\sigma \qquad (24)$$

A continuum study of the texture effect is conductd by varying R and allowing σ in Eq. (9) be replaced by σ_t. The results of this as well as those of n and m variations are discussed later.

Thermal Effects:

An approximate account of heat generation and dissipation during the perforation process has also been made. Short of a complete three-dimensional

heat flow solution, the method adopted here is thought to be reasonably accurate. The entire plastic work increment, $\dot{w}_p$, [Eq. (7)] is assumed to be converted to heat during time, Δt. Thus the rate of temperature rise, $\dot{T}_r$, in each element is given by

$$\dot{T}_r = 2\sigma\dot{\varepsilon}/c\ c_p\ \rho \tag{25}$$

where c = mechanical equivalent of heat, c_p = specific heat and ρ = density. If only adiabatic heating was allowed, after a time Δt, the temperature of the element would have become

$$T^a = T + \dot{T}_r \Delta t \tag{26}$$

However, part of this generated heat is dissipated away from these elements by conduction. An arbitrary boundary is placed at the extremity of the deformation zone (location AA) beyond which temperature is assumed to remain at room temperature (25°C) at all times (see Fig. 22). Only radial heat flow in the outward direction is allowed, since no deformation occurs in this direction. The temperature drop resulting from heat conduction is given by

$$\dot{T}_d = \frac{k \cdot 2\pi(r + y)h_o\ e^{-\varepsilon}(T_{av} - 25)}{(h - y_o - y)\ c_p\rho} \tag{27}$$

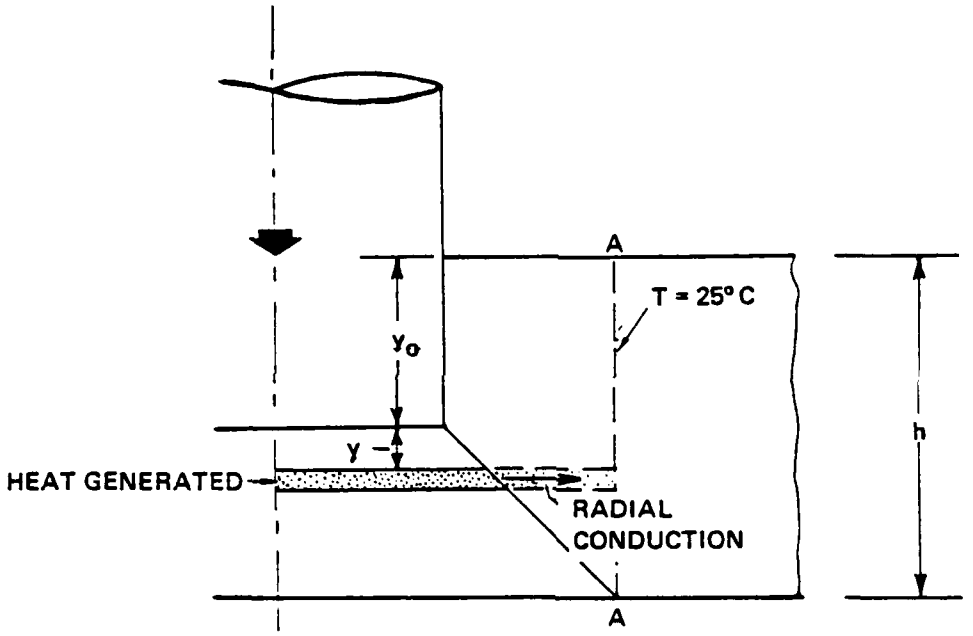

Fig. 22 Schematic diagram illustrating the zone and direction of heat conduction.

where k = conductivity, $T_{av} = (T_\alpha + T)/2$ in centigrade units, h = initial plate thickness and $(h - y_0 - y)$ is the length of the conduction zones at each element location. The net temperature rise (ΔT) is then computed from Eqs. (25) and (27) as follows:

$$\Delta T = (\dot{T}_r - \dot{T}_d)\, \Delta t \tag{28}$$

The influence of this heating effect on local material flow properties is also accounted for in an approximate manner. Literature data[24] on high strength and mild steels indicate a very gradual decrease in flow stress with increase in temperature - nearly a 20% decrease at about 600°C and then a more rapid drop at higher temperatures. The temperature dependence of flow properties is accounted for by allowing K and n in Eq. (18) to be temperature dependent. These functions are approximately described by

$$K_T = K \exp\left\{- 0.000558\ (T-25)\right\}$$
$$n_T = n \exp\left\{- 0.000558\ (T-25)\right\} \tag{29}$$

where K_T and n_T are the K and n values at T°C, K and n being their room temperature values.

Analytical Results

The bulk of the calculations carried out here used values of material properties that are quite representative of 5% Ni steel armor. These were selected as K = 300 ksi, n = 0.05, L = 6 ksi, m = 0.3 with a projectile mass of 0.12 lb. Some calculations were also carried out with L = 2 ksi which indicates a rather low rate sensitivity. Both plate thickness and projectile diameter were chosen to be 0.5 in. Figure 23 shows a plot of how projectile velocity drops during the process of penetration. The initial rapid drop is due to the need for plug acceleration. Low velocity projectiles cannot go past this stage to cause any penetration. Providing initial velocity is sufficiently high, the penetration progresses and subsequent decrease in velocity occurs at an increasing rate. For a 0.5 in. thick plate, it has been assumed that when perforation progresses to the extent of 0.4 in., shear fracture causes plug ejection. This arbitrary fracture criterion is built into the model.

Figure 24 shows the residual velocity of plug and projectile combination as a function of initial plug velocity for a few different anisotropy parameters. The approach to ballistic limit (i.e., zero residual velocity) is clearly marked by a rapid drop in residual velocity from a 45° linear behavior. This simulates observed[18] behavior extremely well.[2] Calculations at and above ballistic limit have shown that melting temperature has been achieved locally. Furthermore, the anisotropy influence on ballistic limit is also seen.

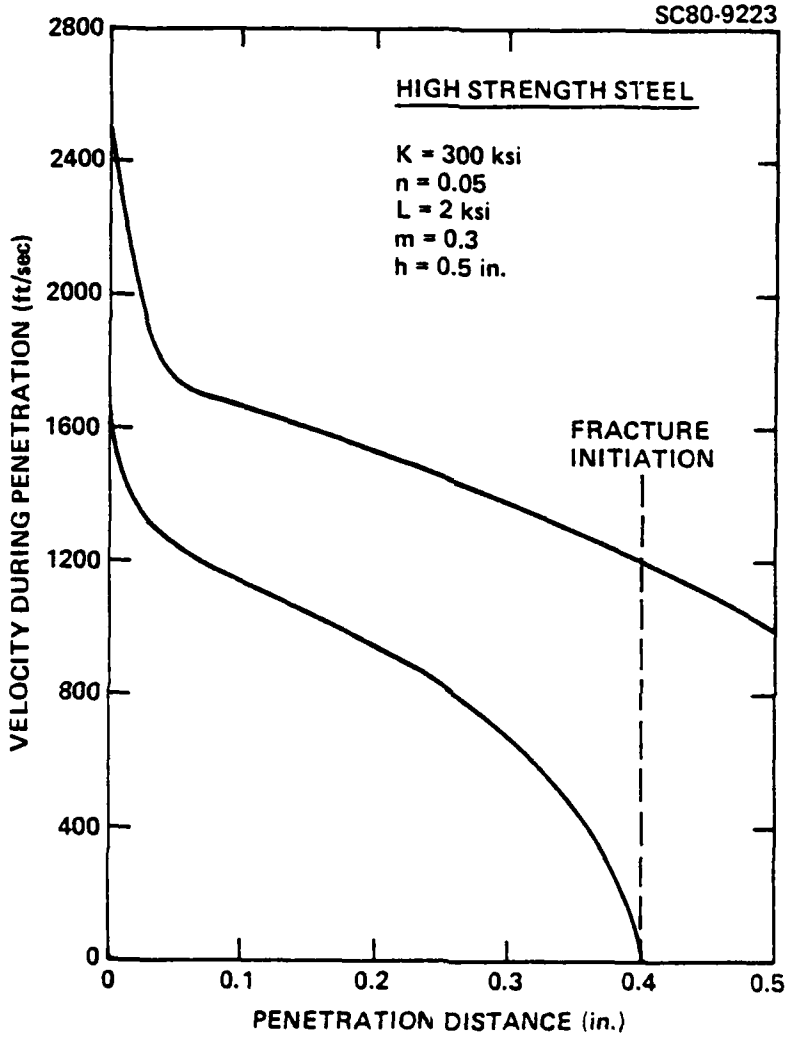

Fig. 23 Change in projectile velocity during ballistic penetration.

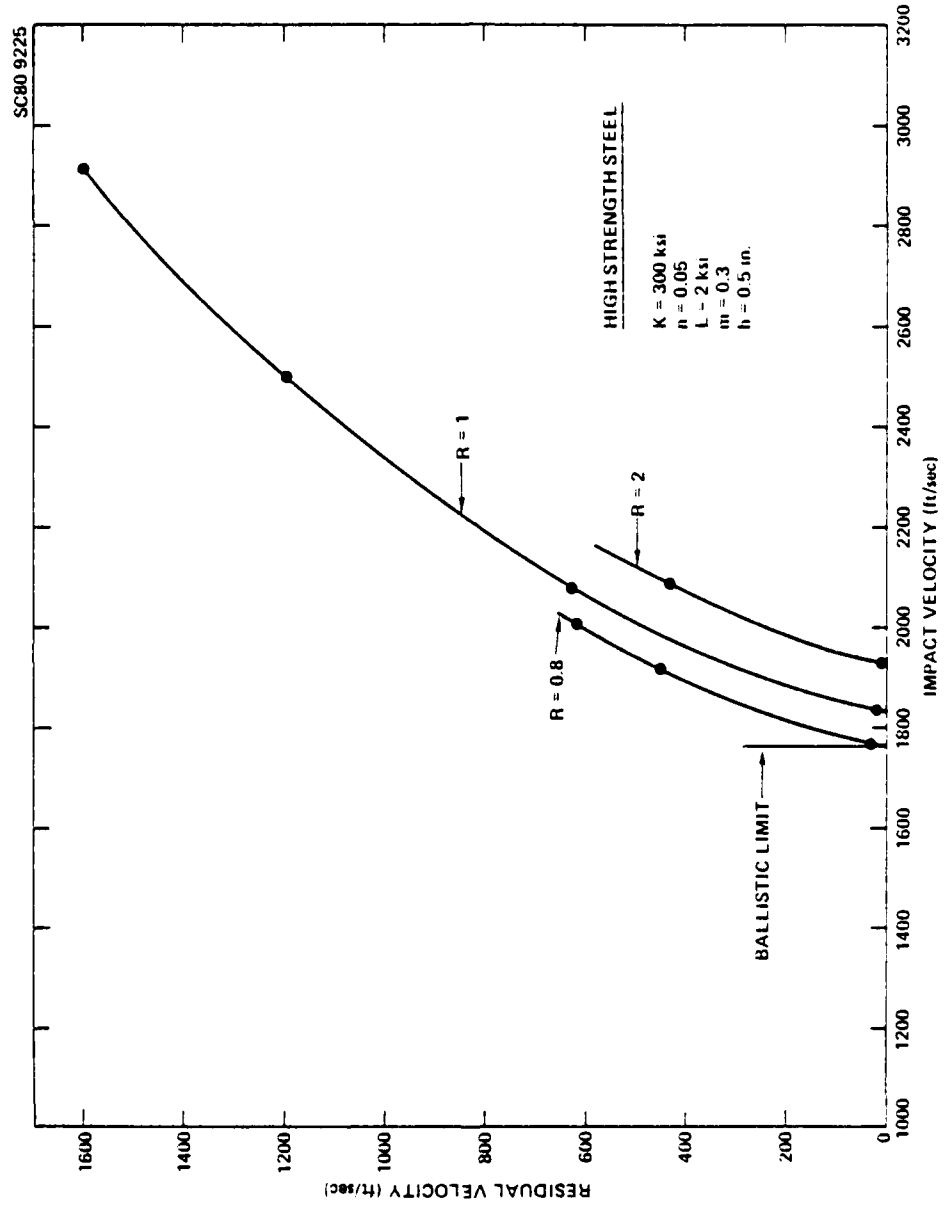

Fig. 24 Residual velocity after plug ejection as a function of initial projectile velocity.

The anisotropy effect and the effect of strain-rate sensitivity are depicted in Fig. 25. There is a 15% rise in ballistic limit in going from R = 0.8 to 2.0. This agrees fairly closely with observed behavior on 5% Ni steel.[3] The influence of strain-rate sensitivity is quite marked because the process requires very high strain rates. Significant improvements are possible from selecting materials with high strain-rate sensitivity, σr, altering microstructure to impart this beneficial property. The influence of strain hardening exponent is shown in Fig. 26. This also acts to increase ballistic limit, however, at the high level of hardness of these armor plates, the effect of strain hardening exponent is somewhat weaker than that of rate sensitivity.

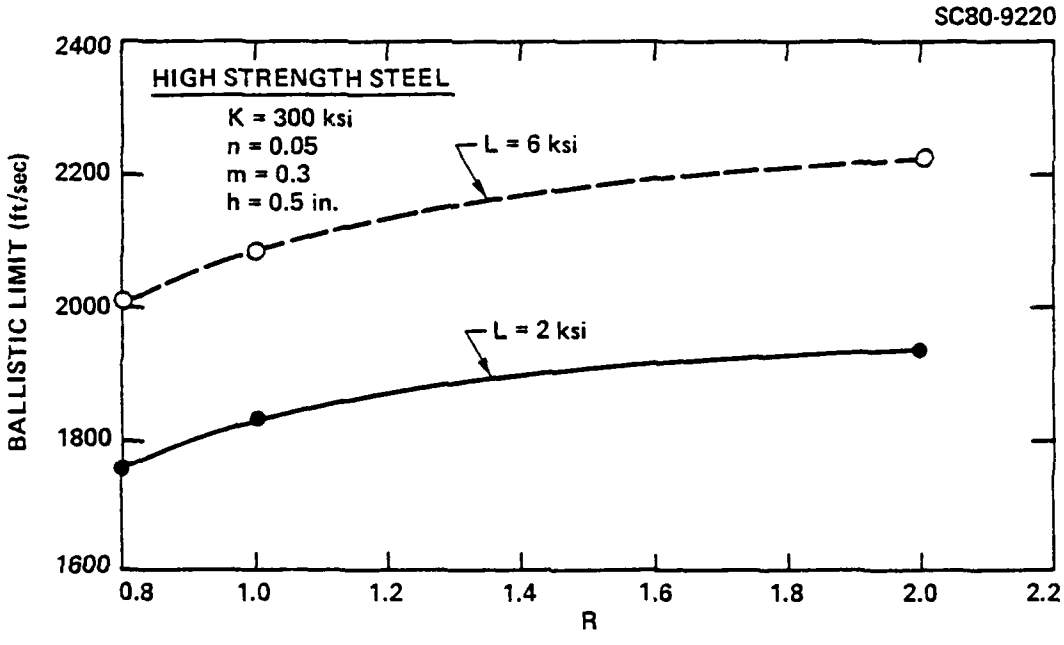

Fig. 25 Improvement in ballistic limit as a function of plactic anisotropy parameter, R, and rate sensitivity constant, L.

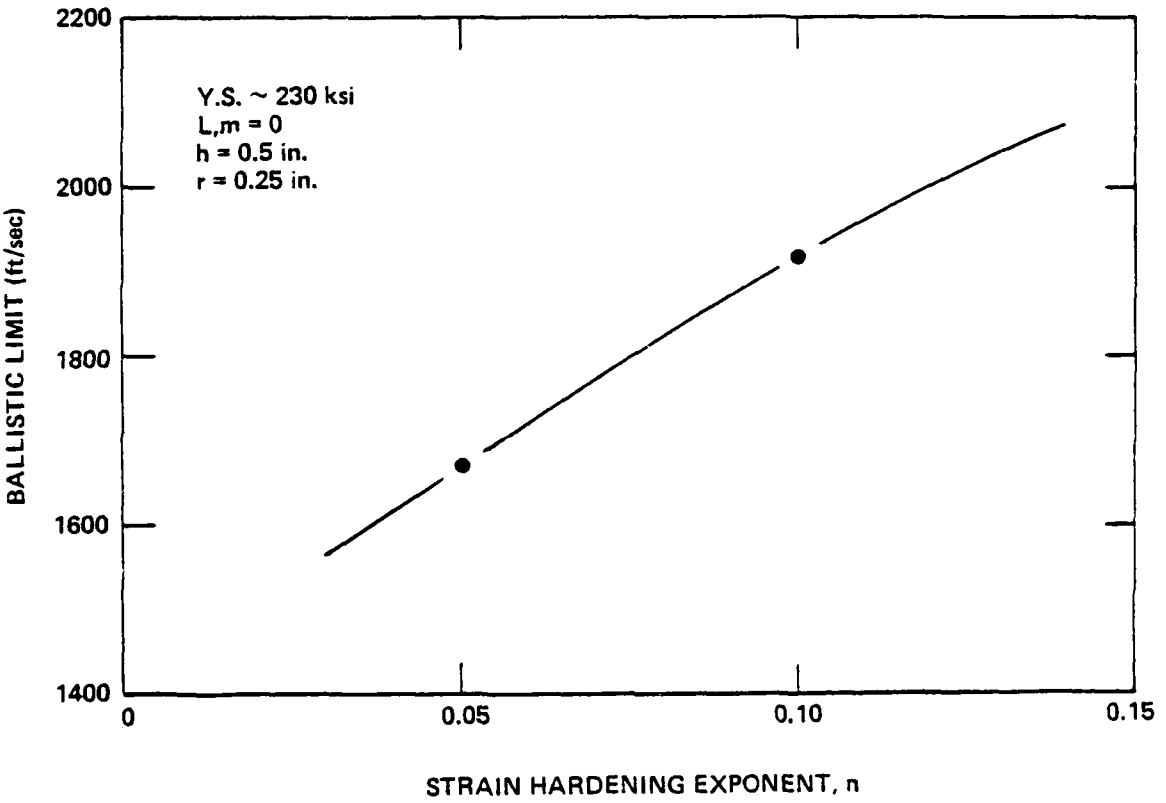

Fig. 26 The effect of strain hardening exponent, n, on ballistic limit.

6.0 SUMMARY AND CONCLUSIONS

Theoretical Taylor factor calculations carried out for a number of f.c.c. rolling (as well as partially recrystallized) textures has indicated that "brass-type" textures, (110) $\langle 1\bar{1}2 \rangle$, are potentially as strong in through-thickness compression as the (111) b.c.c. rolling textures. Since through-thickness strength has been shown to be a strong contributor to ballistic perforation resistance, the development of a high degree of this texture is viewed as quite important. The recrystallization texture, (100) <001>, on the other hand, produces high shear strength but poor through-thickness strength, and is not ideal for ballistic use. In this report, theoretical strength calculations have been carried out not only from ideal textures, but detailed spatial crystallite orientation distribution function has been incorporated in the calculation of Taylor factors. For 7039 aluminum, an armor alloy, these functions were calculated on the basis of their (111) and (200) pole figures, and input into the Taylor factor analysis for a more exact assessment.

An analysis of the ballistic penetration problem has quantitatively validated the importance of plastic anisotropy (due to crystallographic texture) and explained the results observed on 5% Ni steel. Furthermore, the importance of strain hardening and strain-rate sensitivity properties on ballistic limit are also established. Precipitation hardenable austenitic steel, A-286 grade, also included in this study, has shown good promise as an f.c.c. armor material. Some of the important conclusions are listed below:

1. The texture strengthening effect in 7039 aluminum has been found to be extremely small, this is believed to be due to small intensities of "brass-type" preferred orientation achievable in this material.

2. Surface shear strength in 7039 aluminum has been found to be higher than that at the interior, possibly due to a higher cube texture component at the surface.

3. The f.c.c. texture of rolled (900°F and 80°F) A-286 grade high strength steel contains some "brass-type" orientations and appears to be very promising from a ballistic point-of-view.

4. Large anisotropy parameters, R, have been estimated for hot-rolled A286 steel on the basis of compression and shear strength measurements, thereby suggesting improved ballistic resistance.

5. High temperature forming or annealing treatments may significantly reduce the strength and texture intensity of 5% Ni steel.

6. A 15% increase in ballistic limit has been predicted as R is increased from 0.8 to 2.0. This agrees fairly well with observations.

7. Both strain hardening and rate sensitivity enhance ballistic limit. Strain-rate sensitivity has a very strong effect, however, at the high hardness level of armor materials, strain hardening exponents and their effects on ballistic limit are smaller.

7.0 REFERENCES

1. A. K. Ghosh and N. E. Paton, AMMRC Report TR 78-40, September, 1978.

2. Hsun Hu, G. R. Speich and R. L. Miller, AMMRC Report CTR 76-22, July 1976.

3. A. Zarkades, AMMRC Report 79-52, September 1979.

4. G. I. Taylor, J. Inst. Metals, 62, 1938, p. 307; S. Timoshenko, 69th Anniversary Volume, p. 218, McMillan Co., N.Y., 1938.

5. J. F. W. Bishop and R. Hill, Phil. Mag., 42, p. 1298, 1951.

6. W. F. Hosford and W. A. Backofen, Fundamentals of Deformation Processing, W. A. Backofen et al., pp. 259-98, Syracuse Univ. Press, 1964.

7. G. Y. Chin and W. L. Mammel, Trans. Met. Soc., AIME, 239, 1967.

8. G. Y. Chin and B. C. Wonsiewicz, Met. Trans., 1, p. 551, 1970.

9. G. Y. Chin, W. F. Hosford and D. R. Mendorf, Proc. Roy. Soc., A309, p. 433, 1969.

10. R. F. Recht and T. W. Ipson, Trans. ASME, P. 384, Sept. 1963.

11. R. J. Roe, J. Appl. Phys. 36, p. 2024 (1965); 37, p. 2069 (1966).

12. H. J. Bunge, Z. Metallke, 56, p. 872 (1965).

13. P. R. Morris and A. J. Heckler, Advances in X-ray Analysis, 11, p. 454, Plenum Press, New York (1968).

14. G. Wulf, Int. J. Mech. Sci., 20, p. 609, 1978.

15. T. A. C. Stock and K. R. L. Thompson, Met. Trans., 1, p. 219, 1970.

16. E. B. Kula and S. L. Lopata, Trans. AIME-TMS, 215, p. 980, 1959.

17. C. Stickels and P. R. Mould, Met. Trans., 1, p. 1303, 1970.

18. R. L. Woodward and M. E. deMorton, Int. J. Mech. Sci., 18, p. 119, 1976.

19. W. Goldsmith and S. A. Finnegan, Int. J. Mech. Sci., 13, p. 843, 1971.

20. R. L. Woodward, Int. J. Mech. Sci., 20, p. 599, 1978.

21. A. Zarkades and F. Larson, AMMRC, private communication.

22. A. K. Ghosh, J. Mat. Eng. Tech. Trans. ASME, 99, p. 264, 1977.

23. R. Hill, The Mathematical Theory of Plasticity, Oxford Univ. Press, 1967.

24. Mil Handbook, U.S. Dept. of Defense publication, Sept. 1971.

Army Materials and Mechanics Research Center
Watertown, Massachusetts 02172
TEXTURE STRENGTHENING OF PLATES FOR
BALLISTIC PURPOSES, Amit K. Ghosh and
Neil E. Paton, Rockwell International
Science Center, Thousand Oaks, CA 91360

Final Report AMMRC TR 80-45, June 1980, 78 pp-
illus - tables, Contract DAAG46-79-C-0011
D/A Project
Final Report, December 19, 1978 to March 18, 1980

AD _____

UNCLASSIFIED
UNLIMITED DISTRIBUTION

Key Words

Texture
Preferred orientation
Alloy steel
Aluminum alloy
Deformation
Ballistics

Motivated by previous studies in relating texture-based strength to ballistic performance of 5% Ni steel armor, an investigation was initiated to examine other materials, particularly face-centered cubic materials, for possible texture strengthening effects. Theoretical and experimental work were carried out side by side, and significant progress in understanding and achieving that goal are reported here. On the theoretical side, {110} and {111} textures were identified as the most strong contributors to through-thickness strength, and hence ballistic resistance. A computer program to calculate Taylor factors from pole figure data by incorporating spatial crystallite orientation distribution function was developed. Furthermore, theoretical modeling of the ballistic perforation process (Section 5) validated the previously speculated effects of normal anisotropy as well as showed the effects of other material properties, including strain hardening and strain-rate sensitivity. The experimental work on 7039 aluminum indicated only a weak texture and, relative absence of anisotropy leading to an absence significant ballistic effects. (Possibilities of altering this situation has been suggested in the text). Precipitation hardenable austenitic steel, A-286 grade, also used in this work, does give rise to "brass type" texture in rolled (at 80° and 900°F) and aged condition and appears to have a high through-thickness strength needed for ballistic resistance.

Army Materials and Mechanics Research Center
Watertown, Massachusetts 02172
TEXTURE STRENGTHENING OF PLATES FOR
BALLISTIC PURPOSES, Amit K. Ghosh and
Neil E. Paton, Rockwell International
Science Center, Thousand Oaks, CA 91360

Final Report AMMRC TR 80-45, June 1980, 78 pp-
illus - tables, Contract DAAG46-79-C-0011
D/A Project
Final Report, December 19, 1978 to March 18, 1980

AD _____

UNCLASSIFIED
UNLIMITED DISTRIBUTION

Key Words

Texture
Preferred orientation
Alloy steel
Aluminum alloy
Deformation
Ballistics

Motivated by previous studies in relating texture-based strength to ballistic performance of 5% Ni steel armor, an investigation was initiated to examine other materials, particularly face-centered cubic materials, for possible texture strengthening effects. Theoretical and experimental work were carried out side by side, and significant progress in understanding and achieving that goal are reported here. On the theoretical side, {110} and {111} textures were identified as the most strong contributors to through-thickness strength, and hence ballistic resistance. A computer program to calculate Taylor factors from pole figure data by incorporating spatial crystallite orientation distribution function was developed. Furthermore, theoretical modeling of the ballistic perforation process (Section 5) validated the previously speculated effects of normal anisotropy as well as showed the effects of other material properties, including strain hardening and strain-rate sensitivity. The experimental work on 7039 aluminum indicated only a weak texture and, relative absence of anisotropy leading to an absence significant ballistic effects. (Possibilities of altering this situation has been suggested in the text). Precipitation hardenable austenitic steel, A-286 grade, also used in this work, does give rise to "brass type" texture in rolled (at 80° and 900°F) and aged condition and appears to have a high through-thickness strength needed for ballistic resistance.

Army Materials and Mechanics Research Center
Watertown, Massachusetts 02172
TEXTURE STRENGTHENING OF PLATES FOR
BALLISTIC PURPOSES, Amit K. Ghosh and
Neil E. Paton, Rockwell International
Science Center, Thousand Oaks, CA 91360

Final Report AMMRC TR 80-45, June 1980, 78 pp-
illus - tables, Contract DAAG46-79-C-0011
D/A Project
Final Report, December 19, 1978 to March 18, 1980

AD _____

UNCLASSIFIED
UNLIMITED DISTRIBUTION

Key Words

Texture
Preferred orientation
Alloy steel
Aluminum alloy
Deformation
Ballistics

Motivated by previous studies in relating texture-based strength to ballistic performance of 5% Ni steel armor, an investigation was initiated to examine other materials, particularly face-centered cubic materials, for possible texture strengthening effects. Theoretical and experimental work were carried out side by side, and significant progress in understanding and achieving that goal are reported here. On the theoretical side, {110} and {111} textures were identified as the most strong contributors to through-thickness strength, and hence ballistic resistance. A computer program to calculate Taylor factors from pole figure data by incorporating spatial crystallite orientation distribution function was developed. Furthermore, theoretical modeling of the ballistic perforation process (Section 5) validated the previously speculated effects of normal anisotropy as well as showed the effects of other material properties, including strain hardening and strain-rate sensitivity. The experimental work on 7039 aluminum indicated only a weak texture and, relative absence of anisotropy leading to an absence significant ballistic effects. (Possibilities of altering this situation has been suggested in the text). Precipitation hardenable austenitic steel, A-286 grade, also used in this work, does give rise to "brass type" texture in rolled (at 80° and 900°F) and aged condition and appears to have a high through-thickness strength needed for ballistic resistance.

Army Materials and Mechanics Research Center
Watertown, Massachusetts 02172
TEXTURE STRENGTHENING OF PLATES FOR
BALLISTIC PURPOSES, Amit K. Ghosh and
Neil E. Paton, Rockwell International
Science Center, Thousand Oaks, CA 91360

Final Report AMMRC TR 80-45, June 1980, 78 pp-
illus - tables, Contract DAAG46-79-C-0011
D/A Project
Final Report, December 19, 1978 to March 18, 1980

AD _____

UNCLASSIFIED
UNLIMITED DISTRIBUTION

Key Words

Texture
Preferred orientation
Alloy steel
Aluminum alloy
Deformation
Ballistics

Motivated by previous studies in relating texture-based strength to ballistic performance of 5% Ni steel armor, an investigation was initiated to examine other materials, particularly face-centered cubic materials, for possible texture strengthening effects. Theoretical and experimental work were carried out side by side, and significant progress in understanding and achieving that goal are reported here. On the theoretical side, {110} and {111} textures were identified as the most strong contributors to through-thickness strength, and hence ballistic resistance. A computer program to calculate Taylor factors from pole figure data by incorporating spatial crystallite orientation distribution function was developed. Furthermore, theoretical modeling of the ballistic perforation process (Section 5) validated the previously speculated effects of normal anisotropy as well as showed the effects of other material properties, including strain hardening and strain-rate sensitivity. The experimental work on 7039 aluminum indicated only a weak texture and, relative absence of anisotropy leading to an absence significant ballistic effects. (Possibilities of altering this situation has been suggested in the text). Precipitation hardenable austenitic steel, A-286 grade, also used in this work, does give rise to "brass type" texture in rolled (at 80° and 900°F) and aged condition and appears to have a high through-thickness strength needed for ballistic resistance.

DISTRIBUTION LIST

No. of Copies	To
1	Office of the Under Secretary of Defense for Research and Engineering, The Pentagon, Washington, D. C. 20301
12	Commander, Defense Technical Information Center, Cameron Station, Building 5, 5010 Duke Street, Alexandria, Virginia 22314
1	Metals and Ceramics Information Center, Battelle Columbus Laboratories, 505 King Avenue, Columbus, Ohio 43201
	Deputy Chief of Staff, Research, Development, and Acquisition, Headquarters, Department of the Army, Washington, D. C. 20310
1	ATTN: DAMA-ARZ
	Commander, Army Research Office, P. O. Box 12211, Research Triangle Park, North Carolina 27709
1	ATTN: Information Processing Office
	Commander, U. S. Army Materiel Development and Readiness Command, 5001 Eisenhower Avenue, Alexandria, Virginia 22333
1	ATTN: DRCLDC
	Commander, U. S. Army Materiel Systems Analysis Activity, Aberdeen Proving Ground, Maryland 21005
1	ATTN: DRXSY-MP, H. Cohen
	Commander, U. S. Army Electronics Research and Development Command, Fort Monmouth, New Jersey 07703
1	ATTN: DELSD-L
1	DELSD-E
	Commander, U. S. Army Missile Command, Redstone Arsenal, Alabama 35809
4	ATTN: DRSMI-TB, Redstone Scientific Information Center
1	Technical Library
	Commander, U. S. Army Armament Research and Development Command, Dover, New Jersey 07801
2	ATTN: Technical Library
1	DRDAR-SCM, J. D. Corrie
1	DRDAR-LCA, Mr. Harry E. Pebly, Jr., PLASTEC, Director
	Commander, U. S. Army Natick Research and Development Command, Natick, Massachusetts 01760
1	ATTN: Technical Library
	Commander, U. S. Army Satellite Communications Agency, Fort Monmouth, New Jersey 07703
1	ATTN: Technical Document Center

No. of Copies	To
	Commander, U. S. Army Tank-Automotive Research and Development Command, Warren, Michigan 48090
2	ATTN: DRDTA-UL, Technical Library
	Commander, White Sands Missile Range, New Mexico 88002
1	ATTN: STEWS-WS-VT
	President, Airborne, Electronics and Special Warfare Board, Fort Bragg, North Carolina 28307
1	ATTN: Library
	Director, U. S. Army Ballistic Research Laboratory, Aberdeen Proving Ground, Maryland 21005
1	ATTN: DRDAR-TSB-S (STINFO)
	Commander, Dugway Proving Ground, Dugway, Utah 84022
1	ATTN: Technical Library, Technical Information Division
	Commander, Harry Diamond Laboratories, 2800 Powder Mill Road, Adelphi, Maryland 20783
1	ATTN: Technical Information Office
	Chief, Benet Weapons Laboratory, LCWSL, USA ARRADCOM, Watervliet, New York 12189
1	ATTN: DRDAR-LCB-TL
	Commander, U. S. Army Foreign Science and Technology Center, 220 7th Street, N. E., Charlottesville, Virginia 22901
1	ATTN: Military Tech, Mr. Marley
	Commander, U. S. Army Aeromedical Research Unit, P. O. Box 577, Fort Rucker, Alabama 36460
1	ATTN: Technical Library
	Director, Eustis Directorate, U. S. Army Air Mobility Research and Development Laboratory, Fort Eustis, Virginia 23604
1	ATTN: Mr. J. Robinson, DAVDL-E-MOS (AVRADCOM)
	U. S. Army Aviation Training Library, Fort Rucker, Alabama 36360
1	ATTN: Building 5906-5907
	Commander, U. S. Army Agency for Aviation Safety, Fort Rucker, Alabama 36362
1	ATTN: Library, Building 4905
	Commander, USACDC Air Defense Agency, Fort Bliss, Texas 79916
1	ATTN: Technical Library
	Commander, U. S. Army Engineer School, Fort Belvoir, Virginia 22060
1	ATTN: Library

No. of Copies	To
	Commander, U. S. Army Engineer Waterways Experiment Station, Vicksburg, Mississippi 39180
1	ATTN: Research Center Library
	Commander, U. S. Army Environmental Hygiene Agency, Edgewood Arsenal, Maryland 21010
1	ATTN: Chief, Library Branch
	Technical Director, Human Engineering Laboratories, Aberdeen Proving Ground, Maryland 21005
1	ATTN: Technical Reports Office
	Commandant, U. S. Army Quartermaster School, Fort Lee, Virginia 23801
1	ATTN: Quartermaster School Library
	Commander, U. S. Army Radio Propagation Agency, Fort Bragg, North Carolina 28307
1	ATTN: SCCR-2
	Naval Research Laboratory, Washington, D. C. 20375
1	ATTN: Dr. J. M. Krafft - Code 5830
2	Dr. G. R. Yoder - Code 6384
	Chief of Naval Research, Arlington, Virginia 22217
1	ATTN: Code 471
	Air Force Materials Laboratory, Wright-Patterson Air Force Base, Ohio 45433
2	ATTN: AFML/MXE/E. Morrissey
1	AFML/LC
1	AFML/LLP/D. M. Forney, Jr.
1	AFML/MBC/Mr. Stanley Schulman
	National Aeronautics and Space Administration, Washington, D. C. 20546
1	ATTN: Mr. B. G. Achhammer
1	Mr. G. C. Deutsch - Code RW
	National Aeronautics and Space Administration, Marshall Space Flight Center, Huntsville, Alabama 35812
1	ATTN: R. J. Schwinghammer, EH01, Dir, M&P Lab
1	Mr. W. A. Wilson, EH41, Bldg. 4612
1	Ship Research Committee, Maritime Transportation Research Board, National Research Council, 2101 Constitution Ave., N. W., Washington, D. C. 20418
1	Librarian, Materials Sciences Corporation, Blue Bell Campus, Merion Towle House, Blue Bell, Pennsylvania 19422

No. of Copies	To
1	The Charles Stark Draper Laboratory, 68 Albany Street, Cambridge, Massachusetts 02139
	Wyman-Gordon Company, Worcester, Massachusetts 01601
1	ATTN: Technical Library
	Lockheed-Georgia Company, 86 South Cobb Drive, Marietta, Georgia 30063
1	ATTN: Materials and Processes Engineering Dept. 71-11, Zone 54
	General Dynamics, Convair Aerospace Division, P.O. Box 748, Fort Worth, Texas 76101
1	ATTN: Mfg. Engineering Technical Library
1	Mechanical Properties Data Center, Belfour Stulen Inc., 13917 W. Bay Shore Drive, Traverse City, Michigan 49684
1	Dr. Robert S. Shane, Shane Associates, Inc., 7821 Carrleigh Parkway, Springfield, Virginia 22152
	Director, Army Materials and Mechanics Research Center, Watertown, Massachusetts 02172
2	ATTN: DRXMR-PL
1	DRXMR-PR
1	DRXMR-PD
1	DRXMR-AP
10	DRXMR-EM, Mr. A. Zarkades

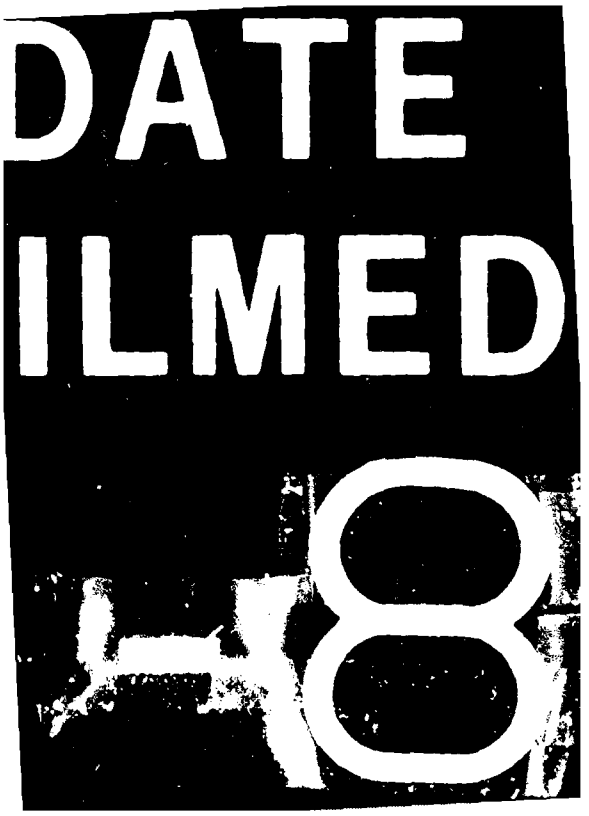
DATE
ILMED
-8